Numerical investigation of tsunami wave impacts on different coastal bridge decks using immersed boundary method

Enjin Zhao [a,b], Junkai Sun [a], Yuezhao Tang [a], Lin Mu [a,b,**], Haoyu Jiang [a,b,*]

[a] College of Marine Science and Technology, China University of Geosciences, Wuhan, 430074, PR China
[b] Shenzhen Research Institute, China University of Geosciences, Shenzhen, 518057, PR China

ARTICLE INFO

ABSTRACT

Due to the strong interaction between the bridges and the extreme waves generated by hurricanes and tsunamis, many coastal bridges were damaged in the past few decades. In this study, in order to investigate the effect of the extreme wave on a bridge, tsunami-like wave generated based on record in the Iwate station during 2011 Japan tsunami event instead of solitary wave is employed to impinge on the bridge with or without air vent. According to the Computational Fluid Dynamics (CFD) theory with a Volume of Fluid (VOF) interface tracking approach, a Numerical Wave Tank (NWT) is developed, in which the Immersed Boundary (IB) method is referred to simulate fluid and structure interaction. The model is calibrated with the experiment. In this numerical tank, the effects of tsunami-like waves with different prominent conditions including wave height and submersion depth on the bridges are studied. Besides, the efficiency of air vent in reducing the hydrodynamic load is also discussed. The results indicate that when the tsunami-like wave overtops the bridges, a noticeable overtopping, where the flow injects into the water fiercely and the whole flow field is very chaotic, is observed. The vertical forces on the bridges are larger than the horizontal forces, leading to many decks to collapse between two piers with small lateral displacement after the hurricanes and tsunamis. After the tsunami-like wave passes over the bridge, the oscillation of the residual wave causes the load oscillation of the bridge. The position of the bridge relative to the initial sea level has a serious impact on the forces on the bridge when the tsunami-like wave passes through it. With the increase of the wave height, the interaction intensity between the tsunami-like wave and the bridge is enhanced and the forces on the bridge also increase, but the effect duration reduces. After the air vent is installed, air vent can reduce the forces on the bridge and improve the efficiency of the bridge protection.

1. Introduction

Coastal bridge as an important tool connecting to lands can be satisfied with the complex coastal transport. However, the bridge structures are very vulnerable to the hydrodynamic and hydrostatic forces. Especially, in the extreme waves during the tsunami and hurricane events, as the sea level increases, the bridge may be partially and fully inundated and air can be trapped causing the external additional force. Once the combined forces exceed the structural bearing capacity of the bridges, the bridges ultimately are damaged (O'Connor and McAnany, 2018). For instance, the 2004 Indian Ocean tsunami resulted in the loss of about half of these bridges along the only road connecting the major Indonesian cities of Meulaboh and Banda Aceh. Similarly, over 300 bridges in the region affected by the tsunami induced by the

2011 Great East Japan Earthquake were either wiped out or damaged beyond repair (Winter et al., 2017). According to the bridge failure reports, when the tsunami impinges on the bridge, the vertical liftoff or overturning of bridge occurs from their substructures to the superstructure, followed by lateral displacement of the superstructure. To understand the mechanism of bridge failure and evaluate potential damage under waves, both physical experiments and numerical simulations have been carried out (Goseberg et al., 2013; Rossetto et al., 2011; Williams and Fuhrman, 2016; Cheng et al., 2018; Crowley et al., 2018).

In some laboratory experiments, the scaled bridge models under wave loads in deep or intermediate water regions were investigated. Seiffert et al. (2015a) conducted a series of laboratory experiments on a 1:35 scale model of a typical two-lane coastal bridge deck using conoidal

---

wave, correspondingly, the same cases are also simulated according to Euler's equations. It is found that the largest vertical uplift and horizontal positive forces occur on the model when the bottom of the deck is just above the water surface. Xiao et al. (2010) investigated the lasting forces impinging on the Biloxi Bay Bridge during Hurrican Katrina by numerical wave model, which indicates that the uplift force on the bridge is greater about 20%–30% than the weight of the bridge deck. Using the smoothed particle hydrodynamic (SPH) method, Sarfaraz and Pak (2017) investigate numerically-derived tsunami wave (solitary wave) loads on bridge superstructures, depending on which simple non-dimensional equations are proposed for computing the tsunami-induced forces and moments to the bridge superstructures.

In order to reduce the wave loads on the bridges, the air vent technology is developed which can release the air pressure. Cuomo et al. (2009) conducted an experimental work at a 1:10 scale physical model in the wave basin of the Yokohama Port and Airport Technical Investigation Office using regular waves. The dynamics of wave-loading of coastal bridges were investigated and "ad-hoc" prediction method of both quasi-static and impulsive wave loads was derived. According to the Green-Naghdi solution for solitary wave surface elevation, Seiffert et al. (2015b) studied wave loading on a coastal bridge deck during a storm through laboratory experiments. It is found that there is a significant reduction in vertical uplift forces when air relief openings are added to the structure, particularly with an ade-quate percentage of air relief opening present. Hayatdavoodi et al. (2014) investigated solitary wave-induced forces on a two-dimensional model of a coastal bridge by conducting laboratory experiments and performing a numerical simulation. The effect of formation of entrapped air pockets on the wave forces is analyzed by considering air pressure relief openings on the deck of the model. As a result, the vertical uplift force is higher than that in the model where wave can push the air out of the chamber. The air pockets have less influence on the horizontal forces.

As discussed in the previous research, to investigate the hydrodynamic characteristics of different bridges subjected to extreme waves, most research uses the solitary or regular wave instead of the real extreme wave for numerical investigations and experimental work, which provides very valuable information about the hydrodynamic characteristics around the bridges (Liang et al., 2013, 2017; Wu et al., 2014; Wang et al., 2018; Xu et al., 2018; Liang et al., 2017). Goring (1979) pointed out that if the propagation distance of tsunami wave is sufficient, the extreme wave may break up into a series of solitary waves theoretically. Besides, solitary wave can propagate with a steady form in deep water. These are why solitary waves have been used in more studies (Zhao et al., 2007; You et al., 2019). However, solitary wave can not evolve into the real-world tsunami wave due to the limitation of the geophysical scale. There are some huge differences between tsunami wave and solitary wave. Madsen et al. (2008) indicated that when the tsunami propagates from the deep ocean to coast, if the front of the tsunami becomes sufficiently steep, the front turns into an undular bore without solitary wave. As the wavelength, period and waveform of solitary wave and tsunami wave are almost completely different, so, solitary wave cannot replace tsunami wave to study the effect of tsunami wave on structures.

In summary, present studies manifest that there are still some deficiencies in the research of bridge damage mechanisms under the action of tsunami wave. Firstly, solitary waves are frequently employed instead of tsunami waves to analyze the effects of the tsunami wave on the bridges (Fang et al., 2018). (Qu et al., 2017a) and (Zhao et al., 2019a) studied the influence of tsunami-like wave and solitary wave on a tiled or suspended marine pipelines, which shows that the hydrodynamic strength of the tsunami-like wave on the pipeline is larger than that under the solitary wave and the flow fields under the tsunami-like wave are more complex. (Zhao et al., 2019b) used a numerical model based on the VOF method to simulate the tsunami-like wave exerting on a seawall, which was more severely damaged by the tsunami-like wave than by the solitary wave. Secondly, when the tsunami wave passes over

the bridge, whether the air vent can effectively reduce the damage of bridges caused by tsunami waves needs to be verified.

In order to fully study bridges under extreme waves, this paper investigates tsunami-like wave impacts on different coastal bridges, the prototype of which is recorded in the Iwate station during the 2011 Japan Tsunami event. This paper is mainly divided into five parts. The second part mainly introduces the generation of tsunami-like wave and wave formulas. In the third part, the numerical models are displayed. The accuracy of the model is verified by the comparison between the experimental and numerical simulation data in the fourth part. The systematic numerical simulations are carried out in the fifth part. In this part, firstly, we compare the different effects of the solitary wave and the tsunami-like wave on the bridges. Secondly, the influences of different tsunami-like waves on the various bridges are analyzed. The sixth part makes a summary of this work and prospects for the future.

2. Generation of tsunami-like wave

When the solitary wave propagates in the constant depth water, the waveform remains unchanged due to two reasons, firstly, the balance between the dispersion and non-linear solitary wave; secondly, the small loss of the wave energy in the simulation (Synolakis, 1987). As similar to the characteristics of the solitary wave, the energy attenuation of tsunami wave is very small and its waveform is basically unchanged after the tsunami wave propagates across the ocean. Although solitary wave can not replace tsunami wave, the waveform characteristics and stability of solitary and tsunami-like waves are similar. In order to derive the theoretical equation of tsunami wave, the solitary wave of the Korteweg-de Vries (KdV) equation is used as the basic wave for the superposition of tsunami wave. With a still water depth h, the surface profile of the solitary wave can be expressed as:

$$\eta(x,t) = H_0 \text{sech}^2[k_0(x - x_0 - c_0 t)] \tag{1}$$

where H_0 is the wave height of solitary wave, $k_0 = (3H_0/4h^3)^{1/2}$ denotes the effective wave number, x_0 is the location of wave crest at $t = 0$, $c_0 = [g(H_0+h)]^{1/2}$ is the wave velocity with the gravitational acceleration value g. The angular velocity and wave period are $\omega_0 = k_0 c_0$ and $T_0 = 2\pi/\omega_0$. The surface profile also can be written as:

$$\eta(x,t) = H_0 \text{sech}^2[\omega_0(x/c_0 - (x_0/c_0 + t))] \tag{2}$$

Based on the concept of N-shaped wave, the temporal evolution of the tsunami wave recorded at Iwate South station during the 2011 Japan Tohoku tsunami is composed of superposition of positive and negative different single solitary waves which is referred to tsunami-like wave. The parametric control for the superposition of the solitary wave determines whether the tsunami-like wave is in good agreement with the real-world tsunami wave. The wave superposition formula is expressed as:

$$\eta(x,t_i) = \sum_{i=1}^{n} \varepsilon_i H_0 \text{sech}^2[\alpha_i \omega_0(x/c_0 - (x_0/c_0 + t_i))] \tag{3}$$

where n is the number of basic waves, ε_i and α_i are the scaling factors for every wave corresponding to the basic solitary wave, which reflects the selected wave height, frequency and period. $t_i = \beta_i T_0$ denotes the beginning time of different waves. The temporal evolution of the tsunami wave can be approximated using Eq. (3) with three sech^2 (*) profiles with $[\varepsilon_1 H_0, \varepsilon_2 H_0, \varepsilon_3 H_0] = [-0.8, 2.2, 5.85]$ m, $[\alpha_1 \omega_0, \alpha_2 \omega_0, \alpha_3 \omega_0] = [0.179, 0.198, 0.653]$ min^{-1} and $[\beta_1 T_0, \beta_2 T_0, \beta_3 T_0] = [9.67, 16.33, 21.63]$ min. Here, $H_0 = 6.7$ m and $T_0 = 17$ min are measured at the GPS-based station (Iwate South) where the still wave depth is 204 m (Chan and Liu, 2012; Qu et al., 2017b).

It is hard to solve the fine CFD model with dense mesh next to bridges using this real case. So, under the condition that the characteristics of tsunami wave remain unchanged, tsunami-like waves are used in this

study depending on the scaling principle as follow.

$$\begin{bmatrix} \varepsilon_1 & \alpha_1 & \beta_1 \\ \varepsilon_2 & \alpha_2 & \beta_2 \\ \varepsilon_3 & \alpha_3 & \beta_3 \end{bmatrix} = \begin{bmatrix} -0.119 & 0.0856 & 6.556 \\ 0.328 & 0.0947 & 8.776 \\ 0.873 & 0.31244 & 10.54 \end{bmatrix} \tag{4}$$

In the simulation, the piston-type wavemaker method is used at the inlet boundary. With the movement of the paddle, the water is compressed and the water level rises. Depending on the different movement velocities of the paddle, different waves can be generated. The velocity u_p of numerical wave paddle can be formulated as:

$$u_p = \sum_{i=1}^{3} c_i \eta_i / (h + \eta_i) \tag{5}$$

3. Numerical solver of fluid domain

In the numerical model, the mesh of the fluid domain is subdivided into the fixed rectangular cells according to the immersed boundary (IB) method. The numerical wavemaker and bridge are fully coupled in the fluid domain by defining the fractional volumes of the objects to cells (Hirt and Sicilian, 1985). The mass and momentum conservation equations in the flow can be expressed as:

$$\nabla \cdot (A\mathbf{u}) = 0 \tag{6}$$

$$\frac{\partial \mathbf{u}}{\partial t} + \frac{1}{V_f} \nabla \cdot (A\mathbf{u}\mathbf{u}) = -\frac{1}{\rho} \nabla \cdot p + \mathbf{g} + \mathbf{F} \tag{7}$$

where ∇ is the gradient operator, $\mathbf{u}$ is the velocity vector, A is the area fraction for fluid in the mesh of Cartesian coordinate system, t is the time, V_f is the volume fraction for fluid, ρ is the density, p is the pressure, $\mathbf{g}$ is the object acceleration vector, $\mathbf{F}$ is the viscous acceleration vector of flow.

According to the volume of fluid (VOF) method, the transportation equation of the free surface between water and air is formulated as:

$$\frac{\partial \gamma}{\partial t} + \frac{1}{V_f} \nabla \cdot (\gamma A\mathbf{u}) = 0 \tag{8}$$

where γ is the water volume fraction in the cell of free surface. $\gamma = 0$, $0 < \gamma < 1$, and $\gamma = 1$ control the different phases of air, interface and water. The viscous acceleration vector $\mathbf{F}$ in three directions of Cartesian coordinate can be written as:

$$\rho V_f F_x = s_x - \left[\frac{\partial}{\partial x} (A_x \tau_{xx}) + \frac{\partial}{\partial y} (A_y \tau_{xy}) + \frac{\partial}{\partial z} (A_z \tau_{xz}) \right] \tag{9}$$

$$\rho V_f F_y = s_y - \left[\frac{\partial}{\partial x} (A_x \tau_{yx}) + \frac{\partial}{\partial y} (A_y \tau_{yy}) + \frac{\partial}{\partial z} (A_z \tau_{yz}) \right] \tag{10}$$

$$\rho V_f F_z = s_z - \left[\frac{\partial}{\partial x} (A_x \tau_{zx}) + \frac{\partial}{\partial y} (A_y \tau_{zy}) + \frac{\partial}{\partial z} (A_z \tau_{zz}) \right] \tag{11}$$

where $s_{(i=x, y, z)}$ is wall stress in x-, y-, and z-directions. τ_{xx}, τ_{xy}, τ_{xz}, τ_{yy}, τ_{yz}, τ_{zz} are the terms of shear stress on the grid surfaces.

In order to calculate the turbulent viscosity μ in the shear stress, two-equation κ-ε turbulence model is introduced as:

$$\frac{\partial k}{\partial t} + \frac{1}{V_f} \left(u A_x \frac{\partial k}{\partial x} + v A_y \frac{\partial k}{\partial y} + w A_z \frac{\partial k}{\partial z} \right) = P_t + G_t + D - \varepsilon \tag{12}$$

$$\frac{\partial \varepsilon}{\partial t} + \frac{1}{V_f} \left(u A_x \frac{\partial \varepsilon}{\partial x} + v A_y \frac{\partial \varepsilon}{\partial y} + w A_z \frac{\partial \varepsilon}{\partial z} \right) = \frac{C_{1\varepsilon} \cdot \varepsilon}{k} (P_t + C_{3\varepsilon} \cdot G_t) + D_\varepsilon - C_{2\varepsilon} \cdot \frac{\varepsilon^2}{k} \tag{13}$$

where k is the turbulent kinetic energy, ε is turbulent energy dissipation rate, u, v and w are the velocities in x-, y-, and z-directions, P_t is the turbulent kinetic energy production, G_t is buoyancy production term, D

and D_ε demonstrate diffusion terms and $C_{1\varepsilon}$, $C_{2\varepsilon}$ and $C_{3\varepsilon}$ are constant values, respectively. The *RNG* κ-ε turbulence model has been successfully employed to investigate the hydrodynamics and loads on different marine structures (Zhao et al., 2018, 2019c).

In this study, the flow characteristics are simulated using the Incompressible Flow Solver with Immersed Boundary (IFS_IB), which we recently developed to solve the governing equations. The numerical solutions and control methods considered in this study are listed in Table 1.

At the bottom of the simulation domain and bridge surface, the nonslip wall conditions are imposed on roughness coefficients. Atmospheric pressure is applied on the top boundary and symmetric boundaries are used at two sides of the simulation domain. Wave absorbing boundary with Neumann conditions is used on the outlet.

4. Model verification

Before the investigation of tsunami-like wave impacts on the bridges, this numerical model needs to be verified to ensure the accuracy of the simulation results. Two verification cases have been implemented, including the wave profile and hydrodynamic loads on the bridges under solitary wave.

4.1. Wave elevation profile

The wave generation is a key technology for this study. To ensure this model can generate the wave accurately and stably, the wave profiles of both solitary wave and tsunami-like wave are verified between the simulation results and the analytical solutions. In the simulation, the length and height of the numerical calculation domain are 1500 m and 20 m, respectively. The still water depth h and wave height H of both waves are 8 m and 2 m, respectively. In the vertical region from 8 m to 10 m where the wave propagates, 50 mesh layers are used. In the whole calculation domain, about 385000 grids are distributed. Due to the movement of the wave generation boundary, the wave level rises and the wave propagates in the numerical wave tank (NWT). The flow field of tsunami-like wave generation is shown in Fig. 1.

After the simulation, the comparisons between numerical results and analytical solutions of tsunami-like and solitary waves are shown in Fig. 2, which indicates that the numerical results match the analytical solutions well on both waves. Besides, the duration of the tsunami-like wave is longer than solitary wave and the energy of the tsunami-like wave is more than solitary wave. The effects of two type waves on the bridges are also different completely, which will be discussed in detail. In a word, this model can generate different waves accurately.

4.2. Hydrodynamic load

Except for the verification of the wave profile, whether this model can predict the hydrodynamic loads on the bridges accurately is also very important to this study. In this section, based on the experiments conducted by Hayatdavoodi et al. (2014), the numerical simulations about solitary wave impinging on the bridges are carried out, the results

Table 1
Numerical solutions and control methods in this study.

Items	Numerical schemes and settings
High-resolution VOF method	Switching Technique for Advection and Capturing of Surfaces (STACS) (Darwish and Moukalled, 2006)
Discretization method	Finite volume method
Scheme for derivatives of time and space	Secondary-order approximation
Resolution for velocity and pressure	Pressure Implicit Split Operator (PISO) (Issa, 1986)
Solution for Poisson equation	Generalized Minimal Residual method (GMRES)

(a) t = 112 s

(b) t = 121 s

(c) t= 125 s

(d) t = 132 s
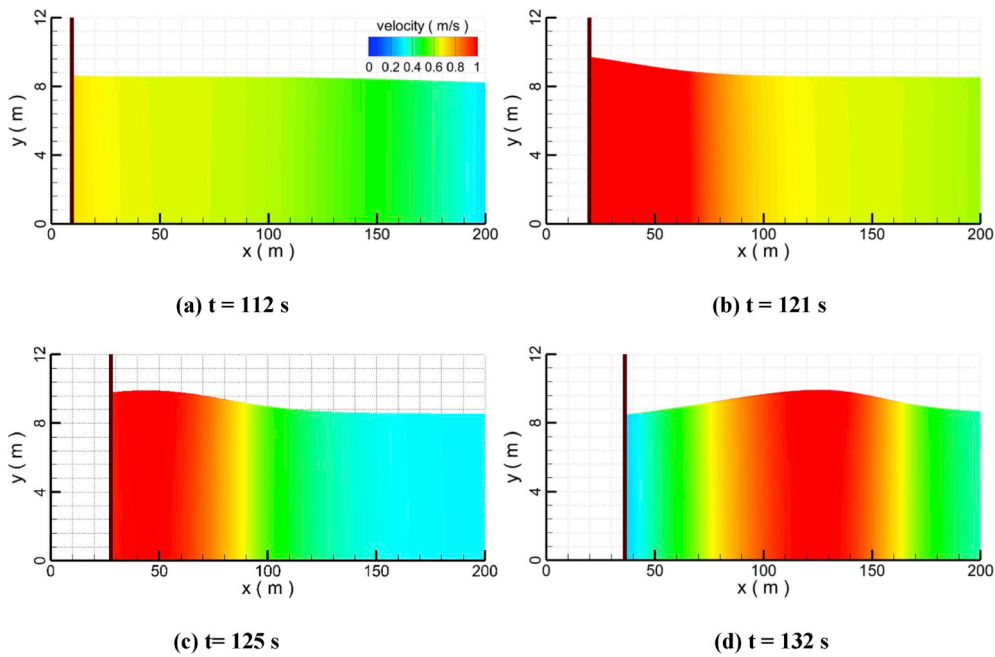
Fig. 1. The flow field of tsunami-like wave generation at different moments.
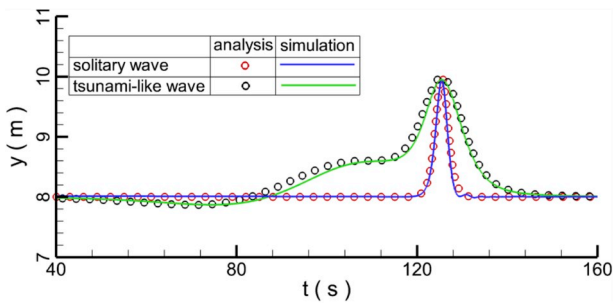
Fig. 2. The wave profile comparison between the numerical results and analytical solutions.

of which are compared with the experimental data to ensure the computing capability of this model. The experimental layout and the bridge configuration are shown in Fig. 3. The experimental bridge is a miniature of the typical coastal bridge after a 1:35 scale.

The whole simulation domain is 10 m in length and 0.26 m in height with three wave elevation gauges (G1, G2, and G3). The wave height and still water depth are 0.0258 m and 0.086 m, respectively. The distance h^* of the upper surface of the deck below the still water level is 0.0172 m. Besides, in order to verify the mesh accuracy of the simulation, three different meshes are used with dense, medium, and coarse meshes consisting of 453,452, 152,482, and 42,156 grids, respectively. When the solitary waves impinge on the submerged bridges, the flow fields and comparisons of wave elevations and hydrodynamic loads on the bridges are shown in Figs. 4 and 5. In every figure about the vorticity or velocity contour of flow field in the following study, the upper figure

(a)

(b)
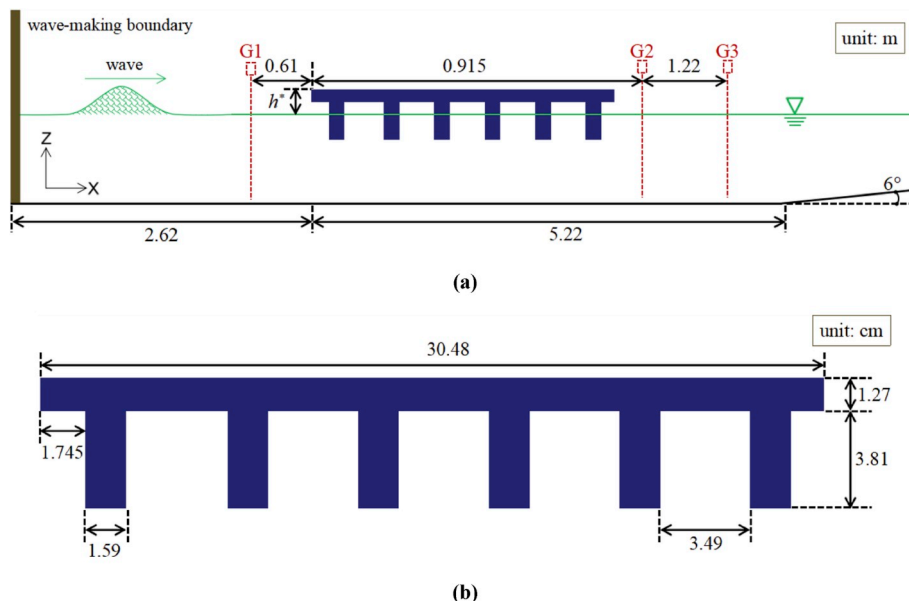
Fig. 3. The experimental layout (a) and configuration of the bridge (b).

is a local flow field around the bridge deck and the lower figure is about a whole flow field that shows the wave propagation position. In the figures, the components (*Fx* and *Fz*) of the hydrodynamic forces in horizontal and vertical directions consist of pressure on the bridge and shear stress along the bridge surface caused by the wave and flow. When the wave approaches and impinges on the bridge, both the horizontal and vertical forces increase to the peak values. After the wave over-topping and leaving, the forces begin to decline and oscillate due to the complex interaction between the wave and bridge, which induces that there is a certain discrepancy between numerical results and experi-mental measurements. Depending on the hydrodynamic load and wave elevation comparisons in Fig. 5, it is found that the simulation results agree with experimental data well for the dense mesh which will be used for the next simulations depending on the scaling principle. This model can generate the wave and calculate the hydrodynamic loads on the bridges accurately.

5. Results and discussion

In this section, the flow fields and hydrodynamic loads on the full-scale bridges (Fig. 6), which scales 35:1 to the model of Fig. 3, under different environmental conditions are investigated and analyzed. *S* denotes the height from the toe of girder to the still water surface, the positive and negative values of which represent the bridge locations corresponding to the still water surface. The length and height of the calculation domain are 800 m and 20 m, respectively. A velocity sensor is located at the point of (x = 41.6 m and z = 2.57 m). The bridge deck is set at 50 m downstream from the wave generation boundary. The hy-drodynamic forces and velocities are normalized as follows:

$$\left(F_x^n, F_z^n\right) = (F_x, F_z) \left/ \left(\rho |\mathbf{g}| a_h a_v l \times 10^{-3}\right)\right. \tag{14}$$

$$(u^n, w^n) = (u, w) / (|\mathbf{g}| a_v)^{1/2} \tag{15}$$

where *u* and *w* are the horizontal and vertical velocities, respectively. a_h, a_v and *l* are the horizontal length, vertical height from the deck surface to the toe of girder and unit width of the deck, respectively. $|\mathbf{g}|$ is the gravity acceleration magnitude.

5.1. Comparison between solitary and tsunami-like waves

Except for the wave profiles of solitary and tsunami-like waves are

different, the flow fields and hydrodynamic loads under two type waves are also investigated and discussed in detail in this section to reveal the essential distinctions of effects of two waves on marine structures. The distance *S* is 1.33 m. The still water depth and wave height of solitary and tsunami-like waves are 8 m and 2 m, respectively. Figs. 7 and 8 show the flow fields of solitary and tsunami-like waves at different moments. When the solitary wave approaches the bridge deck, the water level rises along the front of the deck and the speed of water head increases. Then, the water flows on the top of the deck with the maximum velocity and interlinks with the rising part of rear water at t = 17.10 s, besides, because of the bypass of the bridges, the flow intensity under the girder is also very strong with high flow speed, as shown in Fig. 7c and d. After the wave leaves the bridge deck, the residual water in the deck still flows along the deck due to the inertia effect and drops off the deck behind the bridge at t = 20.10 s and 25.50 s (Fig. 7e and d). Compared with the solitary wave, the duration of tsunami-like wave is much longer and the impact of this wave is even more serious. When the tsunami-like wave overtops the bridges, a noticeable overtopping where the flow injects into the water fiercely and the whole flow field is very chaotic is observed.

The velocities of these two type waves are recorded at the velocity sensor, as depicted in Fig. 9. The title V^n represents the dimensionless velocity including the velocity component (Fig. 9a) and the velocity magnitude (Fig. 9b). The horizontal velocity of the tsunami-like wave is larger than that of solitary wave, however, the vertical velocity of soli-tary wave is larger. Because the vertical velocity is much less than horizontal velocity which plays a leading role in the whole flow field, the velocity magnitude of the tsunami-like wave is larger than that of soli-tary wave (Fig. 9b), leading to the stronger flow under tsunami-like wave. Furthermore, the velocity duration under tsunami-like wave is longer than that under solitary wave, which means that the effective duration of tsunami-like wave on the bridge is much longer.

The temporal evolutions of hydrodynamic loads are displayed in Fig. 10. Before t = 38.5 s, the force components of tsunami-like wave decrease to negative because the leading-depression portion of tsunami-like wave causes the decrease of the water level, the velocity direction reverses to the positive direction of wave propagation. When the pre-ceding elevated portion of tsunami-like wave approaches the bridge deck, the water level and hydrodynamic forces increase and the direc-tion of the horizontal force is consistent with the wave propagation di-rection. When the secondary elevated portion of tsunami-like wave

t = 2.70 s

t = 2.95 s

t = 3.20 s

t = 3.70 s

(a)

(b)

(c)

(d)
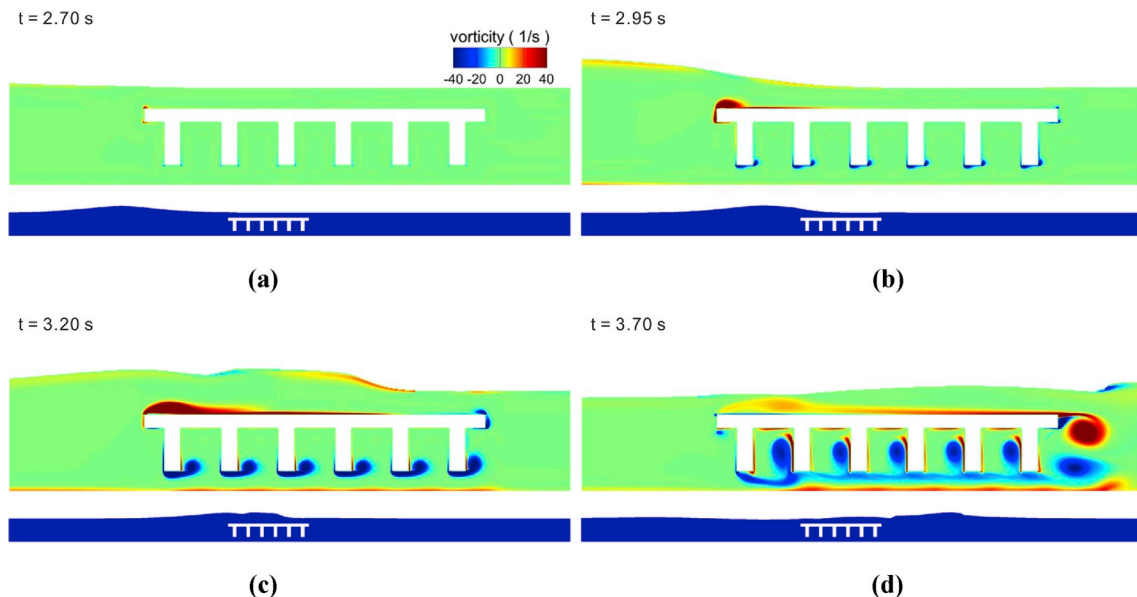
Fig. 4. The flow fields and vorticity contours around the submerged bridges; (a) wave approaching; (b) wave impinging; (c) wave overtopping; (d) wave leaving.
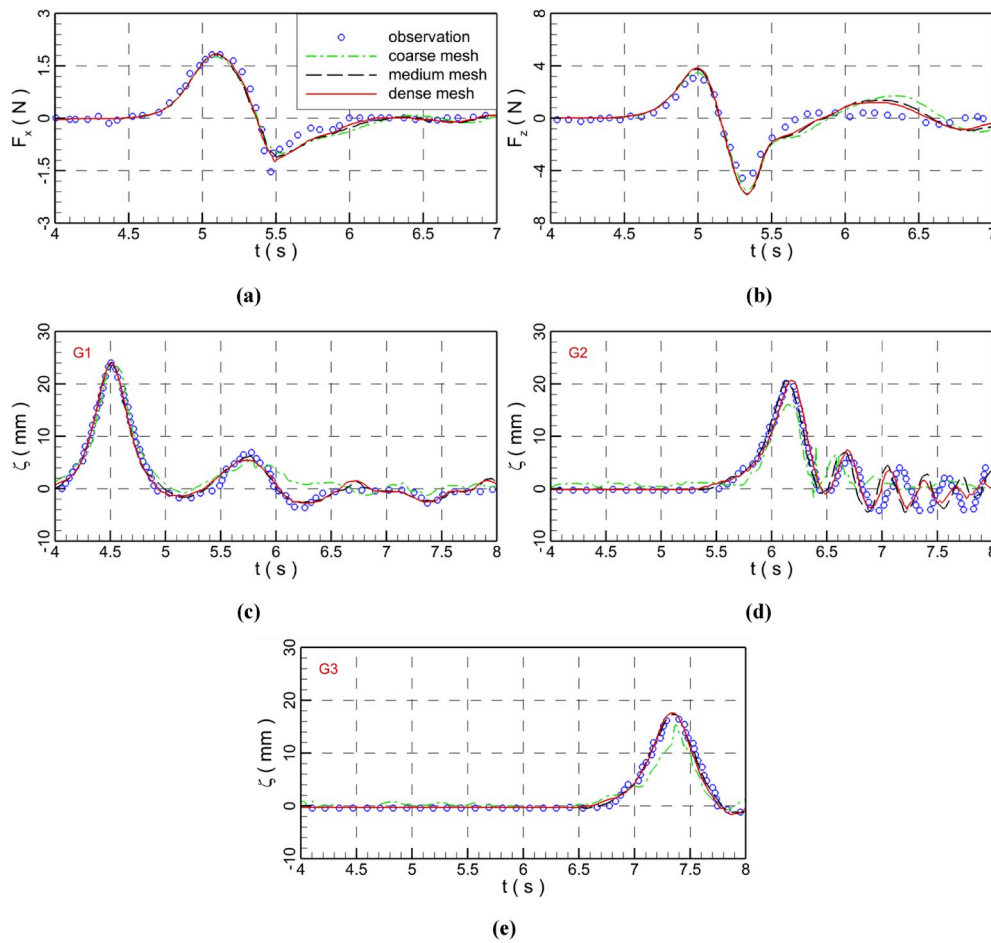
Fig. 5. Comparisons between numerical results and observation for submerged bridges; (a) horizontal loads; (b) vertical loads; (c) (d) (e) wave elevations at G1, G2, and G3.
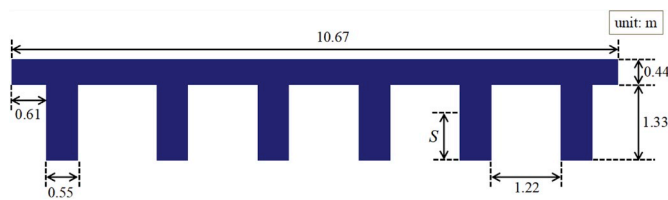
Fig. 6. Configuration of the full-scale bridge deck.

overtops the deck, the wave is broken due to the blocking effect of bridge and much energy contained in the wave releases leading to a great impact on the bridge. The vertical forces on the bridges are larger than the horizontal forces, which is attributed to two reasons. Firstly, when the wave broke, the huge water body in wave portion above the deck with high speed quickly fell on the deck causing the large vertical force. Secondly, the horizontal surface area of the deck is much larger than the vertical area, and the action area of hydrodynamic vertical force is also much larger than that of hydrodynamic horizontal force. These reasons also can explain why many decks collapsed between two piers without lateral displacement after the hurricanes and tsunamis. After the tsunami-like wave passes over the bridge, the oscillation of the residual wave causes the force oscillation of the bridge. Compared with the solitary wave, the effect duration of the tsunami-like wave is much longer and the maximum force is also much larger (Fig. 10b). The bridge will absorb more energy and are more vulnerable to breakage under tsunami-like wave. Therefore, when studying the interaction between bridge and tsunami wave, tsunami wave cannot be simply simplified as

solitary wave.

5.2. Effect of submersion depth

Before the tsunami wave approaches the bridge, the locations of the different parts of the bridge deck relative to the free surface are various along bridge span and in time. The hydrodynamic characteristics around the bridge deck in three different initial states under tsunami-like wave are investigated in this section. The first state is no submersion of the deck where the bottom of girder is above the free surface, and the submersion ratios (α) of submersion depth (S) to wave height H ($H = 2$ m) are -0.50, -0.25 and 0.00, respectively. The partial submersion state is that the free surface is between the top of the deck and the bottom of the girder with the submersion ratios (α) of 0.25, 0.50, 0.67 and 0.75, respectively. The total submersion is with the submersion ratios (α) of 1.00 and 1.25, respectively. The still water depth h is 8 m.

5.2.1. No submersion

The velocity contours of flow fields when the wave impinges on the bridge deck at the time of t = 122 s and 128 s are shown in Fig. 11. When the tsunami-like wave reaches the bridge deck at the same time, with the decrease of the bridge deck position, the intensity of water burst increases and flow velocity gradually decreases. When the wave peak passes over the bridge deck with the submersion ratios of -0.50 and -0.25, the wave head is blocked completely and the wave passes below the bridge. The flow velocity at the bottom of the front girder is the maximum in the whole flow field. The lower the bridge deck, the higher the flow velocity. The minimum velocity of the flow field happens

(a) t = 12.90 s   (b) t = 14.70 s

(c) t= 16.20 s   (d) t = 17.10 s

(e) t = 20.10 s   (f) t = 25.50 s
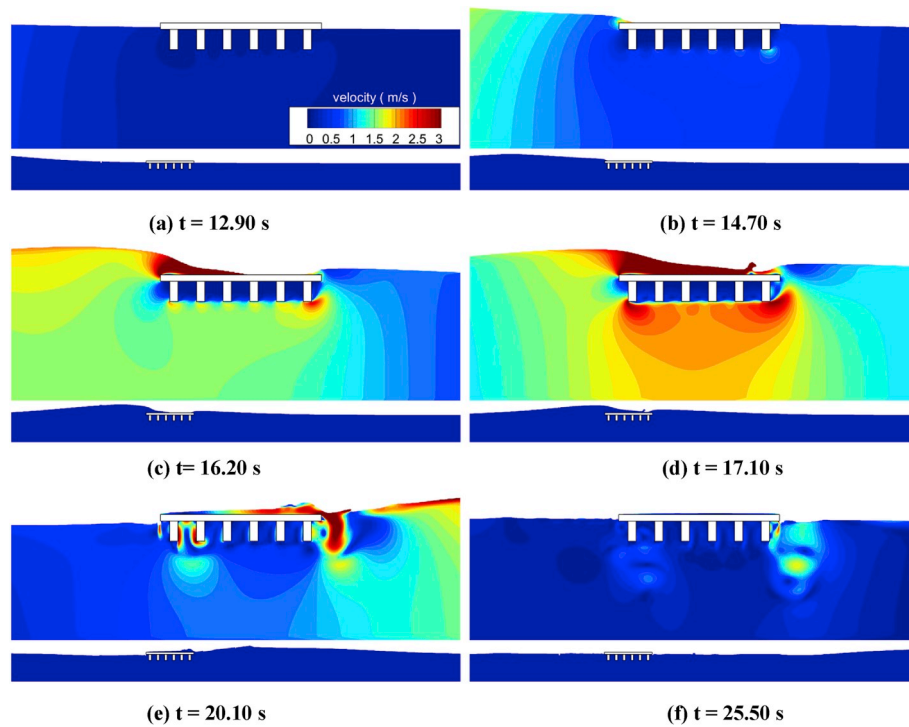
Fig. 7. The velocity contours at different times under solitary wave.

(a) t = 70.00 s   (b) t = 114.00 s

(c) t= 122.00 s   (d) t = 128.00 s

(e) t = 136.00 s   (f) t = 140.00 s
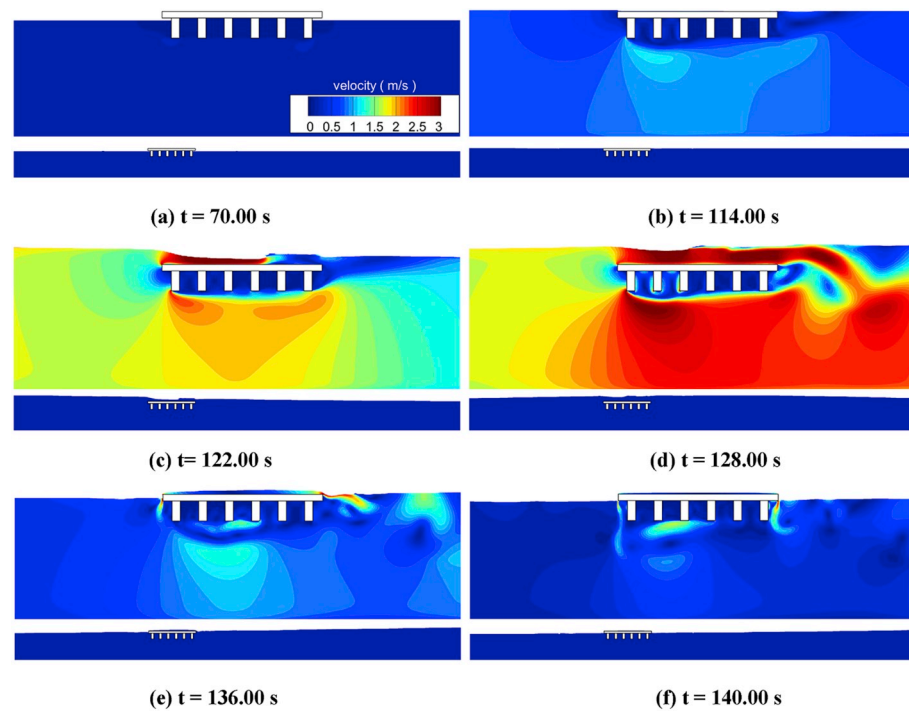
Fig. 8. The velocity contours at different times under tsunami-like wave.

behind the bridge due to the obstruction and bypass effect of the bridge. When the submersion ratio is 0.00 and wave peak is around the bridge deck, some water has passed above the deck surface. The horizontal and vertical hydrodynamic forces on the whole bridge deck are displayed in Fig. 12. The higher the bridge deck, the shorter the duration affected by the wave, because only the water at wave crest can affect the bridge. With the decrease of the bridge deck, both the horizontal and vertical forces on the bridge increase and the duration of the wave effect also

extends.

5.2.2. Partial submersion

When a part of the bridge deck is under the free surface at the initial state, the velocity contours of the flow fields around the bridge deck are shown in Fig. 13. When the wave reaches the bridge deck at the time of 122 s, the velocity around the bridge is smaller than that of other parts in the flow field because of the bridge barrier. When the wave peak arrives
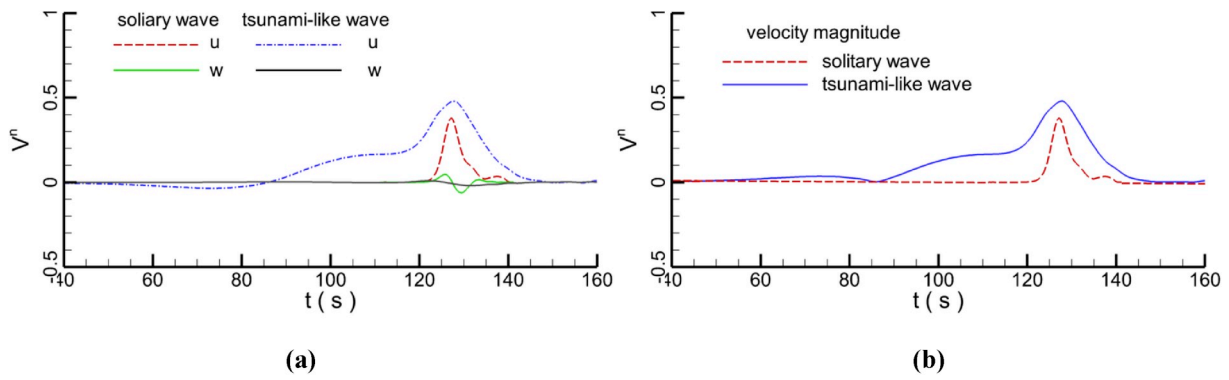
Fig. 9. The temporal evolutions of velocities; (a) velocity components; (b) velocity magnitude.
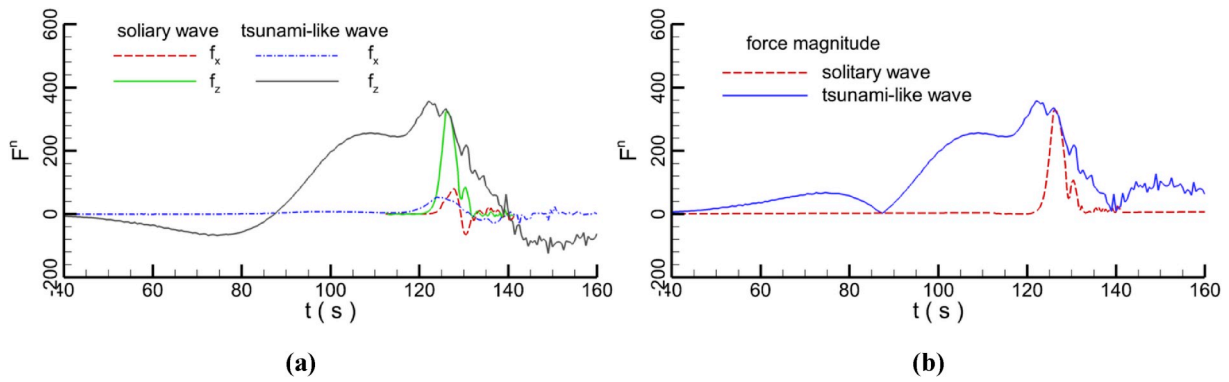
Fig. 10. The temporal evolutions of hydrodynamic forces; (a) force components; (b) force magnitude.
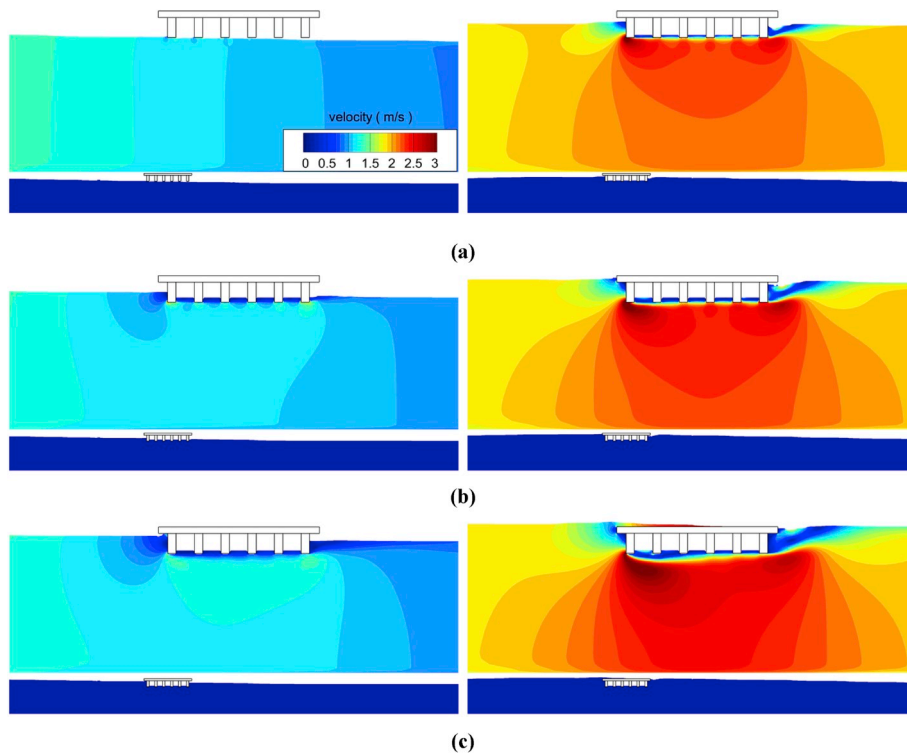
Fig. 11. The velocity contours at times of 122 s and 128 s with different submersion ratio; (a) $\alpha = -0.50$; (b) $\alpha = -0.25$; (c) $\alpha = 0.00$.
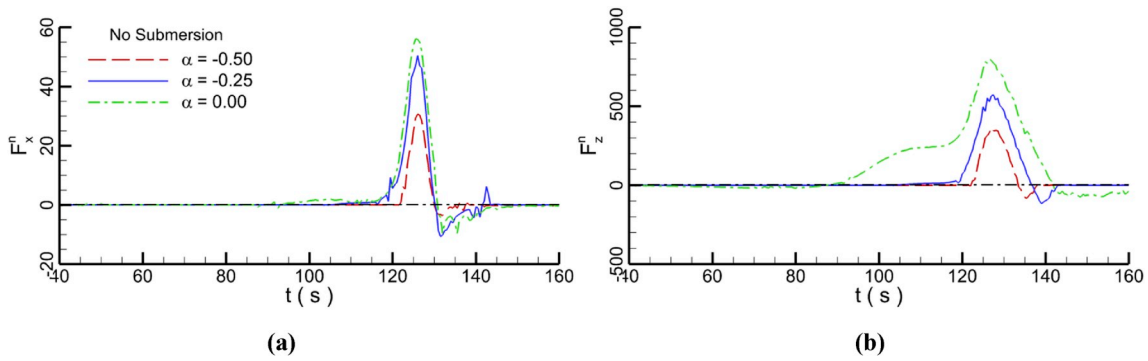
Fig. 12. The temporal evolutions of hydrodynamic forces; (a) horizontal component; (b) vertical component.
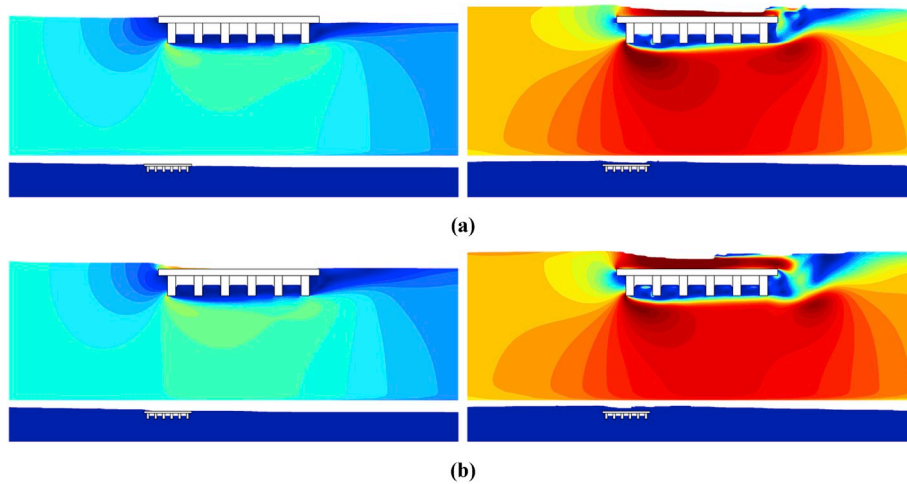
Fig. 13. The velocity contours at times of 122 s and 128 s with different submersion ratios; (a) $\alpha = 0.25$; (b) $\alpha = 0.75$.

at the bridges, some water overtops the bridge deck with high speed and connects with the rising water behind the bridge deck. The flow below the bridge deck also crosses the bridge deck with high speed. However, the velocity of flow among the girders is very small due to the shelter of these girders and some air is trapped in these spaces causing the extra air pressure on the bridge. The hydrodynamic forces on the bridges are drawn in Fig. 14. The horizontal forces on the bridges are similar to each other. After the wave passes over the bridge, the horizontal forces oscillate violently. There are three reasons causing the phenomena. Firstly, when the wave passes through the bridge, the water around the bridge has inertial property and still keeps moving forward, interacting with the bridge; secondly, in the process of water level falling, the flow velocity decreases. Due to the significant change of the flow velocity, the turbulence effect on the bridge is enhanced. At the same time,

considering the inertial motion of the water, the action directions and magnitudes of different parts of the water on the bridge vary greatly. The effect of flow on the bridge becomes chaotic leading to a serious oscillation of the horizontal force on the whole bridge; thirdly, compared with the vertical force, the horizontal force is smaller. The oscillating effect of horizontal force is more serious than that of vertical force. For the vertical forces, with the increase of the submersion depth, the forces decrease because the forces caused by the water above and below the bridge cancel each other out when the wave passes. The deeper the bridge is immersed, the more serious the force offset, and the smaller the vertical force on the bridge deck.

5.2.3. Total submersion

When all the bridge deck has been immersed in the water before the
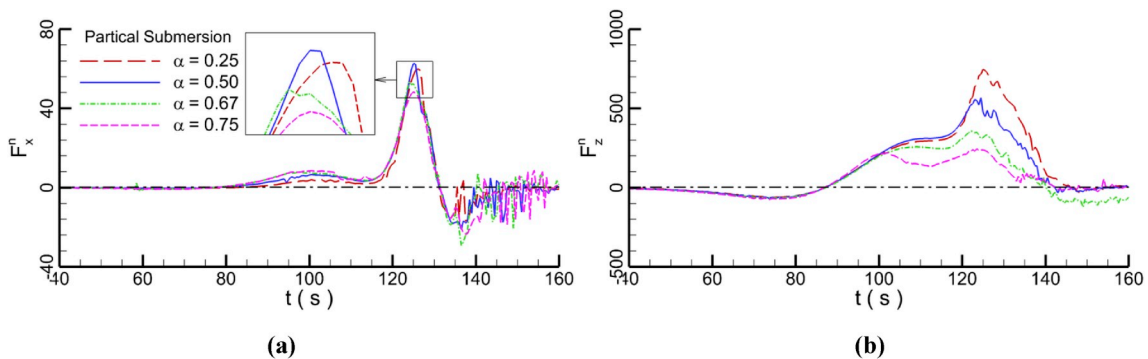
Fig. 14. The temporal evolutions of hydrodynamic forces; (a) horizontal component; (b) vertical component.

tsunami-like wave peak arrives at the bridge deck, the spaces between the girders are filled by the water and the velocity contour of flow field at the submersion ratio of 1.00 is shown in Fig. 15. The flow velocity above the bridge deck is larger than below the bridge deck because when the wave passes over the bridge, the wave breaks and the velocity of upside water of wave is larger than the downside water. Due to the obstruction of the girders, the flow velocity among the girders is much small. When the submersion ratio is 1.25, the vorticity contour of the flow field is displayed in Fig. 16. When the leading-depression portion of the tsunami-like wave approaches the bridge, the water level decreases and the flow direction is toward wave inlet, so there are some vortices in front of girders and deck. When the preceding elevated portion arrives at the bridge deck, the water elevation increases and the fluid flows downstream, inducing that the vortices around the bridge shed downstream. With the increase of the water level, the fluid velocity increases and the vortexes behind the bridge also gradually increase. The water in the spaces among the girder also is disturbed by the bottom flow and some vortices are generated along the surfaces of the girders. Then, some vortices shed behind the bridge. When the wave peak reaches the bridge, the bridge looks like a whole barrier to block the flow. The bigger vortices are generated and shed behind the bridge. The hydrodynamic forces on the bridge are shown in Fig. 17. With the increase of submersion depth, both the horizontal and vertical forces decrease because the upper velocity of the tsunami-like wave is larger than the lower velocity. The temporal evolutions of the horizontal forces are basically consistent with the waveform. The oscillations of the vertical forces are more serious than that of the horizontal forces because the length of the whole bridge is much longer than the height. The vertical forces on the horizontal surface of the bridge are much larger than the horizontal forces on the vertical surface. So, the influence of flow on vertical force is more serious than that on the horizontal force. When the wave passes through the bridge, the interaction between the wave and bridge causes the water to oscillate and the forces on the bridges also vibrate. The more serious the oscillation of flow is, the more severe the oscillation of vertical force is. Therefore, the oscillations of forces in the vertical direction are much stronger than that in the horizontal direction.

The maximum and minimum hydrodynamic forces at three different states on the bridges are depicted in Fig. 18. Here, as noted above, a negative horizontal force means the force in the opposite direction of the wave propagation, and a negative vertical force implies a downward force. For the horizontal hydrodynamic force, in the state of no submersion, with the increase of the submersion depth, the maximum forces increase and minimum forces decrease, which means that the horizontal force magnitude increase due to the increase of the action area of wave on the bridge. In the state of partial submersion, when the submersion ratio is less than 0.5, with the increase of the submersion depth, the hydrodynamic force still increases because the turbulent flow caused by the wave breaking is strengthened, leading to a great impact on the bridge. However, when the submersion ratio is larger than 0.5, the force decreases because the velocity at the bottom of the wave is smaller than that at the top, the deeper the immersion depth, the smaller the wave influence. With the weakening of the interaction between waves and bridges, the horizontal forces reduce. Similar to the horizontal forces, in the state of no submersion, with the increase of the submersion depth, the magnitude of vertical hydrodynamic forces increase. When the toe of the bridge deck is lower than the still water level, the vertical forces

decrease with the increment of the submersion depth. It is deduced from the results that if the bridge has been immersed below the water level before the wave crest reaches the bridge, the damage to bridge will be greatly reduced with the increase of immersion depth.

5.3. Effect of wave height

In this section, the effects of the tsunami-like waves with different wave heights on the bridge are investigated to real the hydrodynamics around the bridge under the various marine conditions. The still water depth is 8 m and seven wave heights with $H = 1.4, 1.6, 1.8, 2.0, 2.2, 2.4$ and 2.6 m are considered in the simulations. The distance from the still water surface to the toe of the girder is 1 m. Although only the change of wave height, it is actually the relative change of the wave height (H) to the still water depth (h) in the governing equations of wave generation and propagation, such as the effective wave number and wave propagation velocity, and the wave height of the tsunami-like wave is coupled with the water depth. The ratio β of wave height (H) to the still water depth (h) represents the relative position between the bridge and the shore. The still water depth does not change, but the ratio β is always changing, indicating that the location of the bridge and terrain are constantly changing. For example, both wave length and duration of tsunami-like wave at $\beta = 0.2$ with wave height of 1.6 m are longer than that at $\beta = 0.325$ with the wave height of 2.6 m, which conforms to the law of the wave propagation in deep water. In deep water, the tsunami wave height is smaller, but the wavelength and duration are longer. When the tsunami wave propagates to the offshore area, the shoaling effect on the wave is significant at $\beta = 0.325$. The wave energy gathers, the wave height becomes higher, and the wavelength and duration become shorter. The higher the ratio β, the closer the wave is to the shore, which means the bridge is close to the shore.

The wave profiles with different wave heights recorded in the x = 10 m are shown in Fig. 19. The lower the wave height, the longer the wave duration, which follows the law of wave propagation from deep water to shallow water. When different tsunami-like waves reach the bridge, the velocity contours of flow fields at three moments are shown in Fig. 20. When the crests of the preceding elevated and the secondary elevated wave portions reach the bridge, the velocity contours of flow fields are recorded at the first and second moments, and after the tsunami-like wave leaves, the velocity contour is recorded at the third moment.

At the first moment, with the increase of wave height, the velocity in the whole flow field increases and the maximum speed is about 1.2 m/s. Due to the wave height is less than the bridge height, the wave rises along the bridge and maximum flow velocity appears at the toe of the first girder. The flow velocity below the bridge is larger than other parts of the flow fields because, at a certain water volume, the cross-sectional area of the flow decreases inducing that the velocity of fluid increases. When the crest of secondary elevated wave portion reaches the bridge at the second moment, the wave overtops the bridge with high speed. The higher the wave height, the larger the speed, and more water flows above the bridge surface. After the water body above the bridge passes through the bridge surface, it connects and injects into the rising water causing the intense water fluctuation. Some water in the spaces among the girders oscillates with the low speed because of the shelter of the girders. Besides, it is noted that with the increase of the wave height, the flow velocity increases obviously. After the crest of the tsunami-like
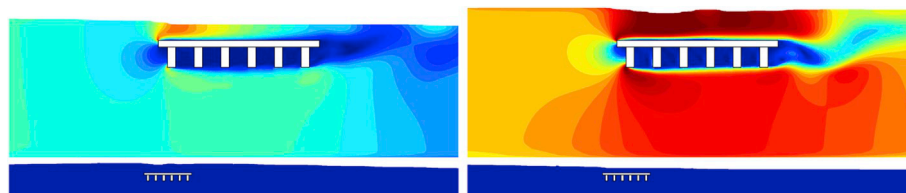
Fig. 15. The velocity contours at times of 122 s and 128 s at the submersion ratio $\alpha = 1.00$.

(a) t = 70.00 s

(b) t = 114.00 s

(c) t= 122.00 s

(d) t = 128.00 s

(e) t = 136.00 s

(f) t = 140.00 s
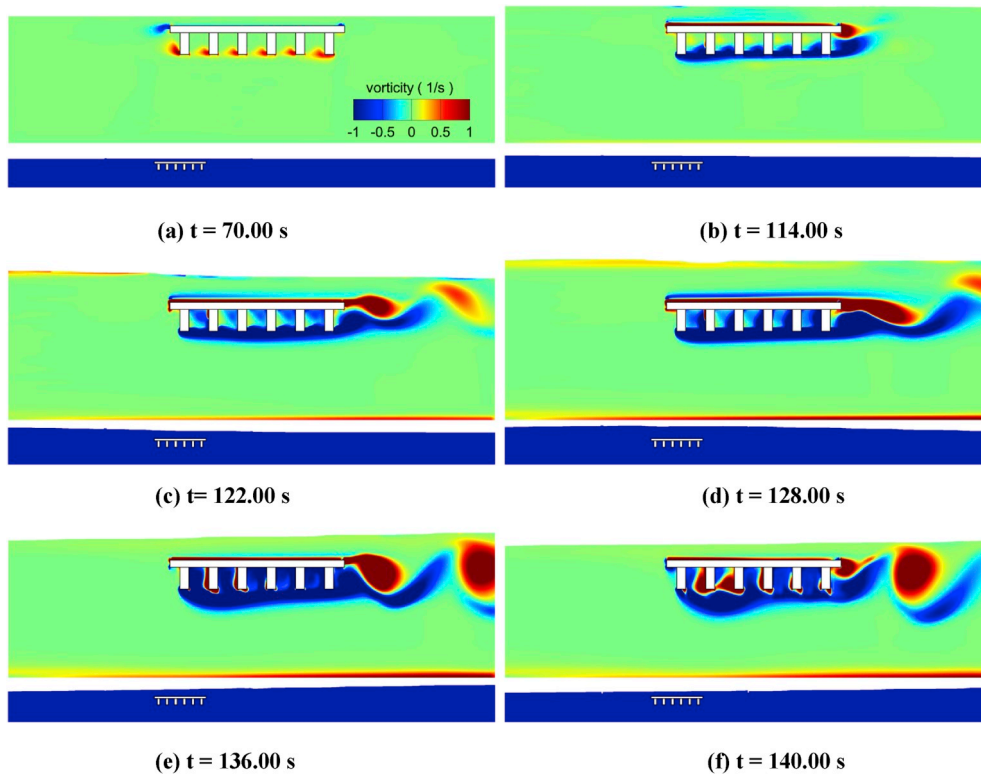
Fig. 16. The vorticity contours at different times at the submersion ratio $\alpha = 1.25$.

(a)

(b)
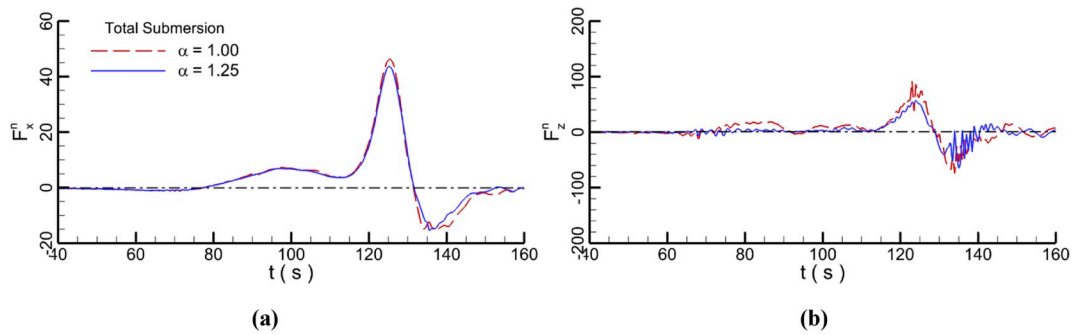
Fig. 17. The temporal evolutions of hydrodynamic forces; (a) horizontal component; (b) vertical component.

(a)

(b)
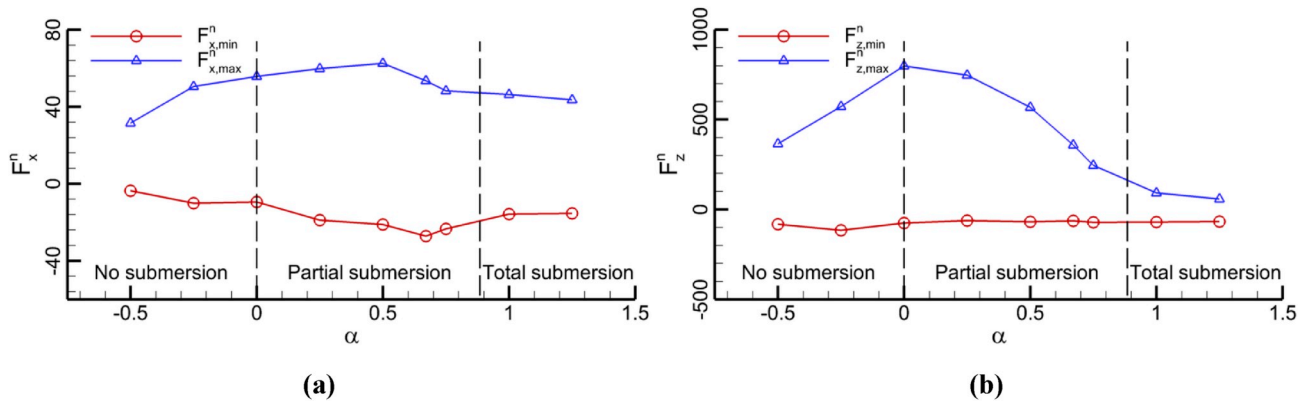
Fig. 18. Maximum and minimum hydrodynamic forces on the bridges at different submersion depths; (a) horizontal forces; (b) vertical forces.
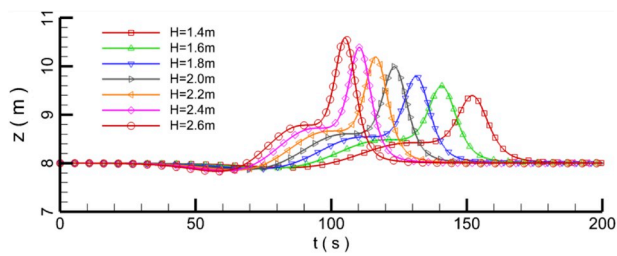
Fig. 19. Wave profiles with different wave heights.

wave passes over the bridge, there are some vortices around the bridge due to the interaction between the water and the bridge. The flow velocity is also much lower than that at the second moment. In conclusion, with the increase of the wave height, the flow velocity increases and the interaction intensity between the flow and bridge also increases, which causes the bridge to be damaged easily.

The temporal elevations of the hydrodynamic forces on the bridges in horizontal and vertical directions are drawn in Fig. 21. With the propagation of the wave, the horizontal hydrodynamic forces increase to the maximum, then, the forces decrease after the tsunami-like wave passes over the bridge. At the leading-depression portion of tsunami-like
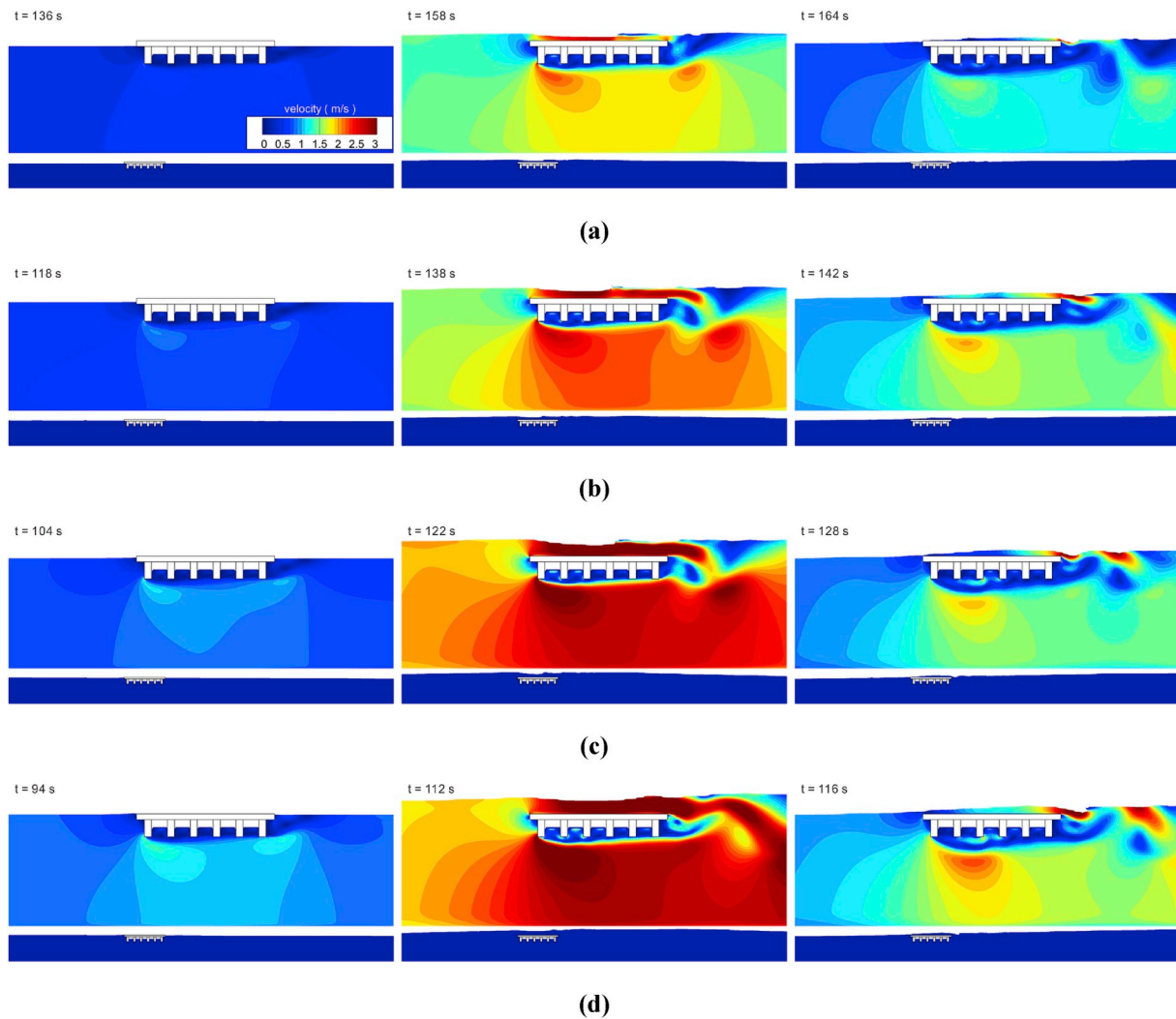
Fig. 20. The velocity contours at three moments with different wave heights; (a) $H = 1.4$ m; (b) $H = 1.8$ m; (c) $H = 2.2$ m; (d) $H = 2.6$ m.
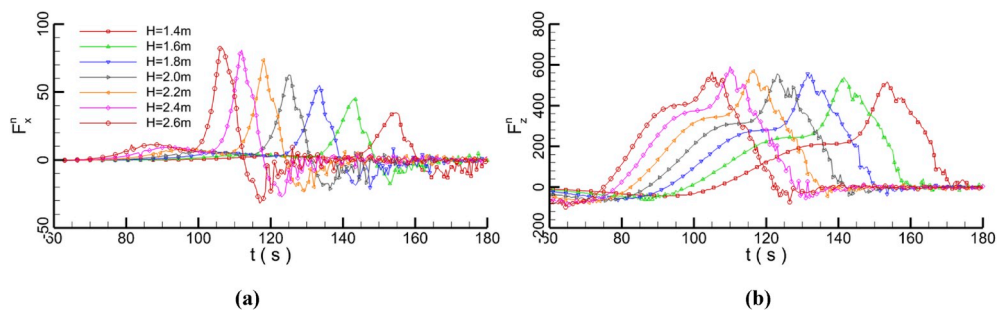
Fig. 21. The temporal evolutions of hydrodynamic forces; (a) horizontal component; (b) vertical component.

wave, some water refluxes causing the horizontal hydrodynamic force is in the negative direction and the force value is less than zero. Besides, the pattern of the horizontal force matches the wave profile well. With the increase of the wave height, the horizontal forces increase but the action duration of the forces on the bridge reduces, which is related to the wave period. In Fig. 21b, when the leading-depression portion approaches the bridge, the water level decreases inducing the decrease of the vertical hydrodynamic force. The lower the wave height, the smaller the vertical force magnitude at this stage. With the wave propagating, the vertical forces increase following the preceding elevated portion of tsunami-like wave. It is noted that the temporal evolutions of vertical force and preceding elevated wave portion coincide with each other, which means that the bridge can not change the waveform at this stage. When the secondary elevated wave portion reaches the bridge, the wave is broken by the interference of bridge which has been immersed in the water completely. The vertical force caused by the bottom water under the bridge is larger than that caused by the top water. Due to the shelter of the girders, the flow in the spaces among the girders is very weak and similar to each other under different wave heights, causing that the vertical forces on the bridges are similar.

The maximum and minimum forces on the bridges are recorded and displayed in Fig. 22. With the increase of the wave height, the horizontal force magnitude including the positive and negative forces increases, which basically shows a linear growth. The magnitude of the positive force is much larger than that of the negative force. When the ratio β is larger than the 0.275, with the increase of the wave height, the raise gradient of horizontal forces decreases. As for the vertical forces, with the increase of the wave height, the maximum force on the bridge increases slowly. In total, with the increase of the wave height, the interaction intensity between the tsunami-like wave and the bridge is enhanced and the forces on the bridge increase, but the effect duration reduces. The higher the wave height, the easier the bridge will be damaged.

5.4. Effect of air vent

In order to reduce the pressure of air tracked among the girders on the bridge, air vent as a good method has been adopted in some bridges (Fig. 23). In this section, the influence of the solitary and tsunami-like waves on the bridges with or without air vent is investigated. The still water depth and wave height are 8 m and 2 m, respectively. The schematic of the bridge deck with the air vents simplified as straight passages is shown in Fig. 24. The size g_s of the air vent is calculated as:

$$g_s = \frac{\varepsilon A_s}{m} \tag{16}$$

where ε is the influence factor for the air exchange rate defined as 0.2, m is the number of the chambers among the girders.
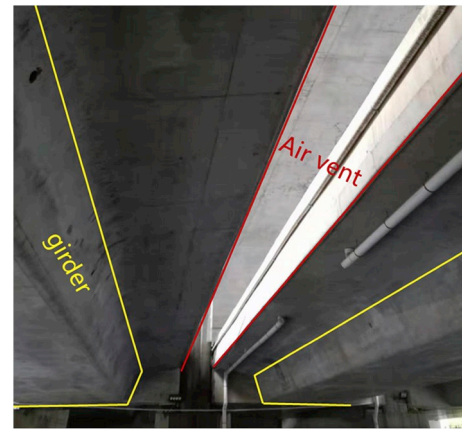
Fig. 23. The air vent in the bridge deck.

Fig. 24. The schematic of the bridge deck with the air vents.

5.4.1. Comparisons under solitary and tsunami-like waves

In this section, the simulations of solitary wave and tsunami-like wave on the bridges with the air vent are conducted and the comparisons of the flow fields and hydrodynamic loads under two waves are analyzed. The submersion depth from the toe of the girder to the still water surface is 0.5 m. The velocity contours of the flow fields under solitary and tsunami-like waves are shown in Figs. 25 and 26. When the wave approaches the bridge, the water level increases and the air in the chamber is compelled to the atmosphere. The velocity around the bridge also increases to the maximum when the wave crest arrives. After the wave leaves the bridges, the flow velocity decreases, and the water in the chamber falls off inducing the oscillation of the flow field. The interaction between the water and the bridge becomes chaotic. Compared with the solitary wave, the volume of high-velocity fluid under tsunami-like wave is much larger, which means that the tsunami-like wave has a serious effect on bridges, as shown in Figs. 25c and 26c. When the wave leaves, it can be seen that the bridge has a significant blocking effect on solitary wave, and the water levels in front of and behind the bridge drop obviously (Fig. 25d), but the propagation of tsunami-like wave is relatively less affected by the bridge. Meanwhile, the flow on the bridge deck drops through the air vent and due to the closure of the chamber, the water inside flows slowly.

When the wave passes through the bridge, the temporal evolutions of forces on the bridges are shown in Fig. 27. The horizontal force under

(a)

(b)
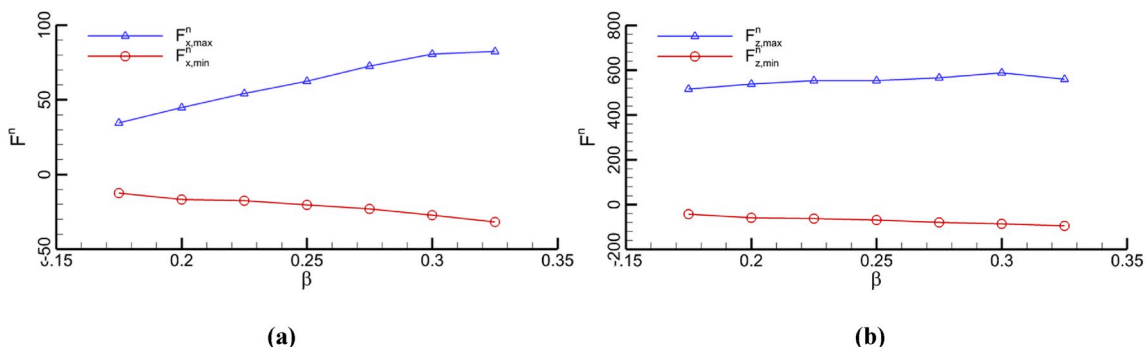
Fig. 22. Maximum and minimum hydrodynamic forces on the bridges at different wave heights; (a) horizontal forces; (b) vertical forces.
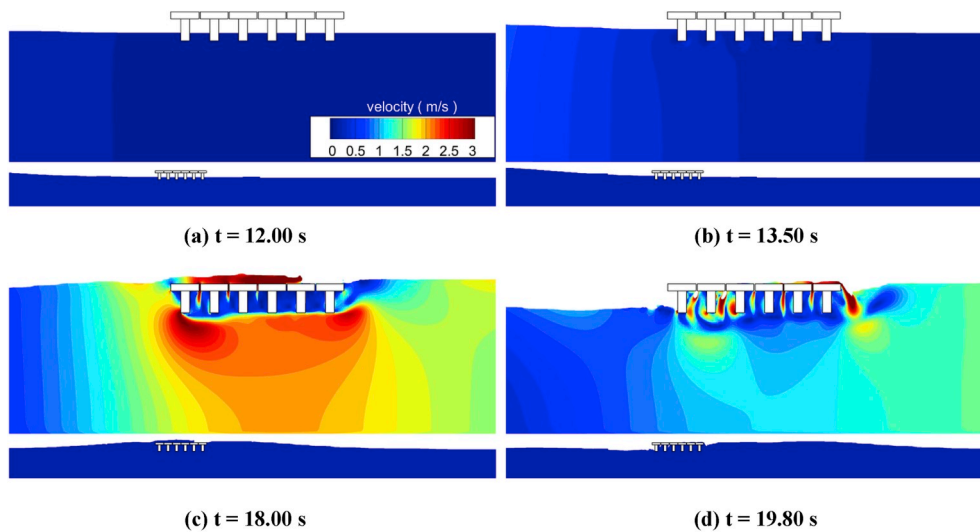
Fig. 25. The velocity contours of flow fields at different moments under solitary wave.
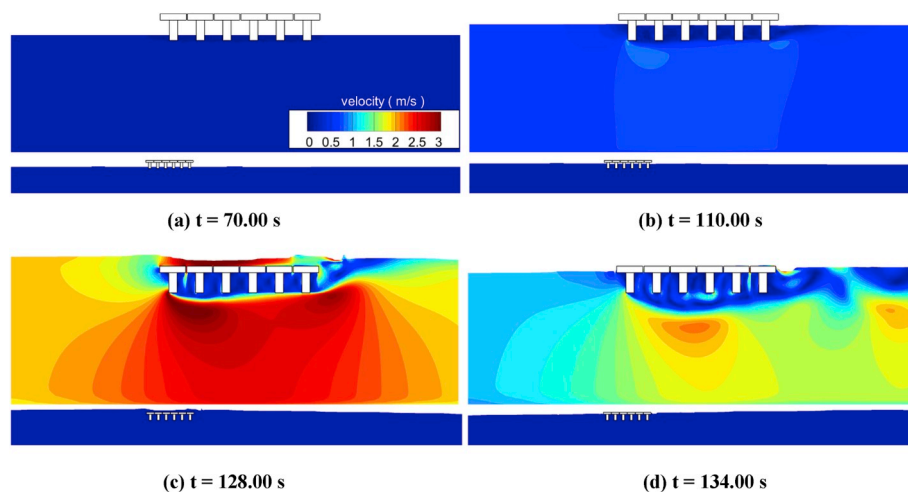
Fig. 26. The velocity contours of flow fields at different moments under tsunami-like wave.

the tsunami-like wave is similar to that under the solitary wave, but the effect duration of tsunami-like wave is much longer. After the wave passes, the oscillation of the water leads to the strengthening of the interaction between the water and the bridge. The forces vibrate violently, as shown in Fig. 27a. The vertical force is larger than the horizontal force for both solitary and tsunami-like waves. The maximum vertical force under the tsunami-like wave is also larger than that under the solitary wave because the tsunami-wave is with a higher velocity and more water (Fig. 27b). The total force magnitudes under two waves are compared in Fig. 27c, which shows that the force under the tsunami-like wave on the bridge with the air vent is still larger than that under the solitary wave even if the air vent exists in the bridge.

5.4.2. Comparisons with and without air vent

Due to the existence of the air vent, the air can be discharged from the chamber. The effects of the tsunami-like waves on the bridge with and without air vent are investigated to real the influence of the air vent on the bridge. The submersion depth from the toe of the girder to the still water surface is 0.5 m. The vorticity contours of flow fields at four moments for two cases with and without air vent are depicted in Figs. 28 and 29. When the preceding elevated wave portion arrives (Figs. 28b and 29b), the air in the chamber without the air vent is compressed and the water level difference exists inside and outside of the chamber. When

the bridge is with the air vent, the air is ejected to the atmosphere through the air vent. With the increase of the water level, the flow passes through the bridge deck. The above air is always trapped in the chamber of the bridge without air vent, and some below flow in the chamber is whirling. However, for the bridge with the air vent, the water fills the chamber after the air is evacuated. At the junction of water bodies around the air vent, some pairs of vortices roll in the chambers, the intensity of which decreases from the first air vent to the last air vent because both the water volume and velocity decrease. After the wave leaves, there are some vortices shedding behind the bridge deck, but the whirling intensity of the flow around the bridge with air vent is much stronger than that of the bridge without air vent. Due to the existence of the air vent, the flow change is much different from that without air vent.

The temporal evolutions of forces on the bridges with and without air vent are shown in Fig. 30. The horizontal forces on the bridges with and without air vent are similar to each other, indicating that the air vent has a weak effect on the horizontal forces. However, the vertical force on the bridge with air vent is much less than that on the bridge without air vent because the vent can release the additional air pressure on the bridge with air vent, which means that the air vent plays a significant role on the protection of the bridge. Since the vertical force is much larger than the horizontal force, the vertical force dominates the overall force on the
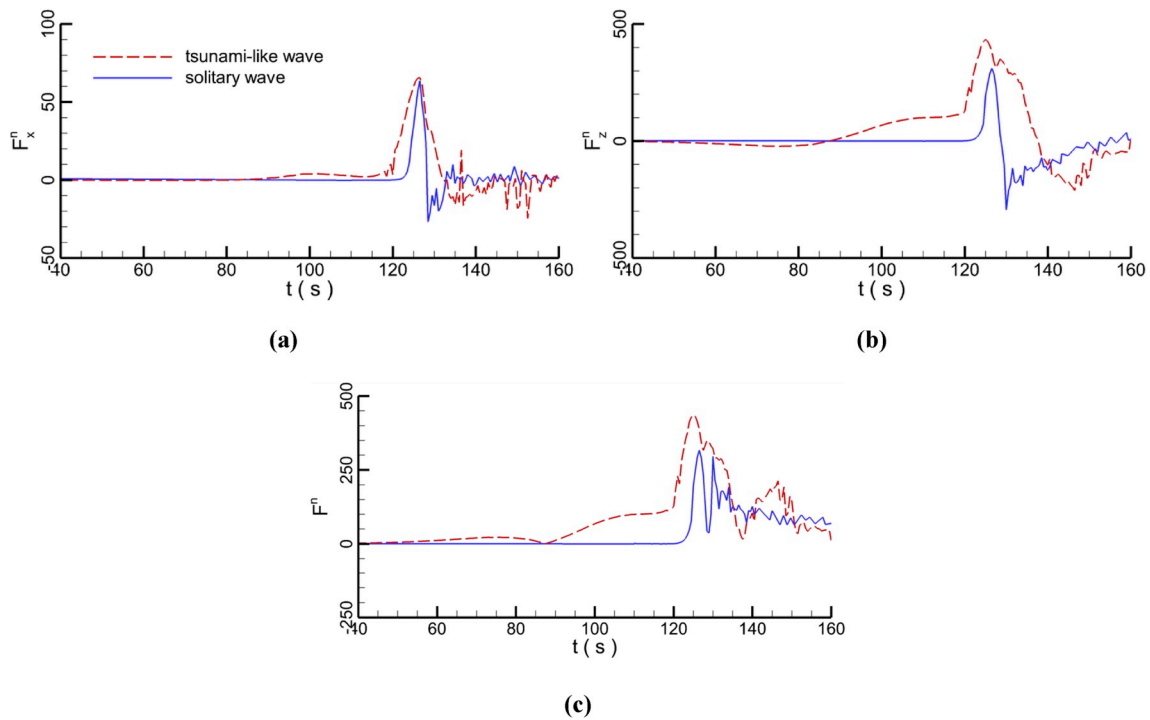
Fig. 27. The forces on the bridge with air vent under the solitary wave and tsunami-like wave; (a) horizontal forces; (b) vertical forces; (c) total force magnitudes.
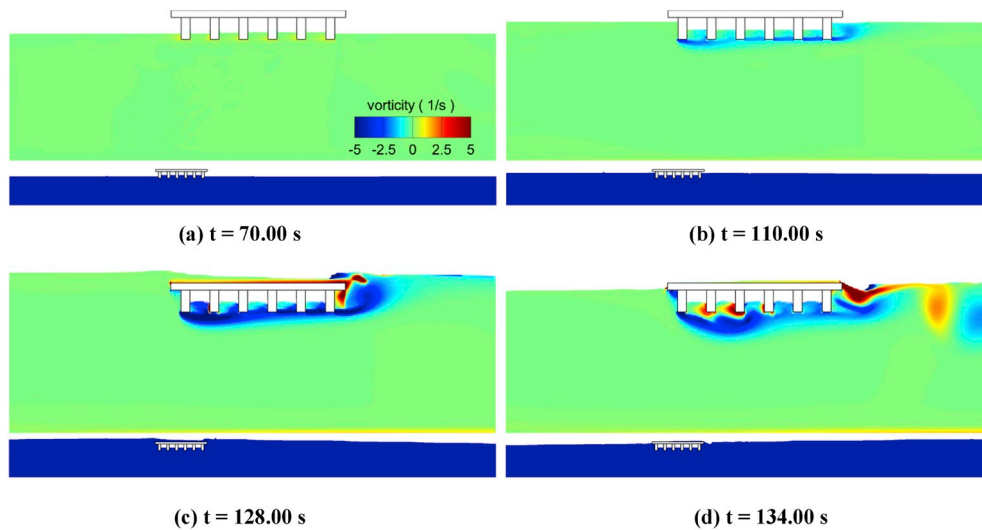
Fig. 28. The vorticity contours of flow fields at different moments under solitary wave.

bridge.

5.4.3. Comparisons under different locations

The effects of air vent on the bridges at different locations are investigated in this section. The submersion depths from the toe of the girder to the still water depth are considered as 0.0, 0.5 and 1.0 m, respectively. The vorticity contours at four moments are shown in Figs. 31 and 32, when the peaks of the leading-depression, the preceding elevated and the secondary elevated wave portions reach the bridge deck and the tsunami-like wave leaves the bridge deck. When the sub-mersion depth is 0.0 m, at the initial stage, the toe of the girder touches the still water surface. When the leading depression wave portion rea-ches the bridge deck, the water level reduces and the water in the interface between the bottom of girders and water drops from the bridge deck causing some weak vortices (Fig. 31a). At the second moment,

some vortices are generated behind every girder and the maximum vorticity occurs at the last girder. With the propagation of the wave, the water level increases and the air is expelled from the chambers through the air vent. When the peak of the secondary elevated wave portion is around the bridge at the third moment, some water flows along the bridge surface and when the water passes through the air vent, a part of it flows or drops into the vent connecting with the elevated water level. Clearly, the biggest vortices happen behind the bridge deck. After the wave leaves, the water level decreases and some water in charmers drops due to the atmospheric connectivity through the air vent. There is still strong turbulence in the water. Compared with the submersion depth of 0.0 m, with the increase of the submersion depth, the intensity of vortices increases (Fig. 32). In the third moment, more water passes over the bridge surface, vortex separation appears at the bridge surface and the air vent. A pair of big vortices shed from the bridge, as shown in
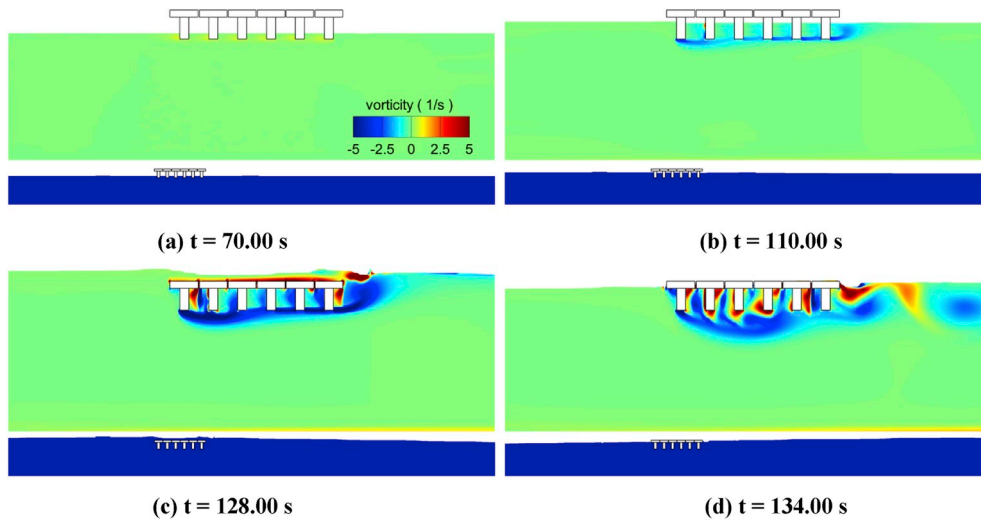
Fig. 29. The vorticity contours of flow fields at different moments under tsunami-like wave.
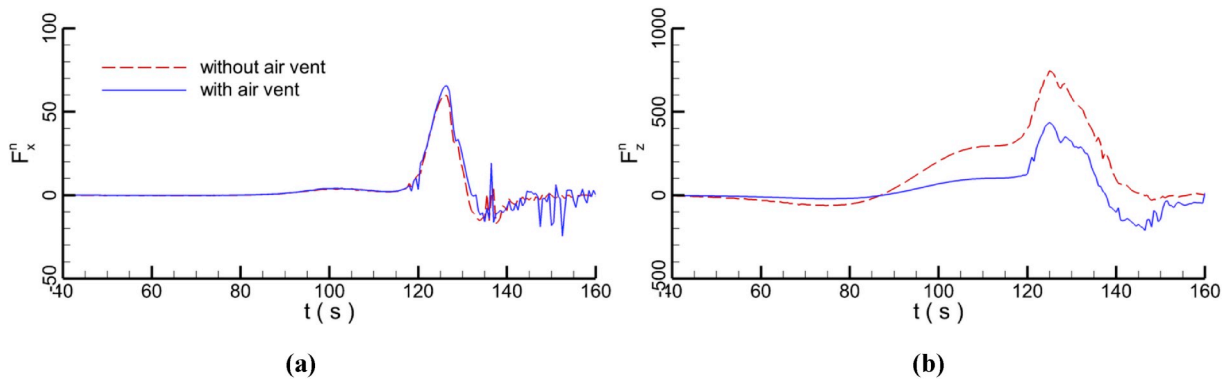
Fig. 30. The forces on the bridge with or without air vent; (a) horizontal forces; (b) vertical forces.
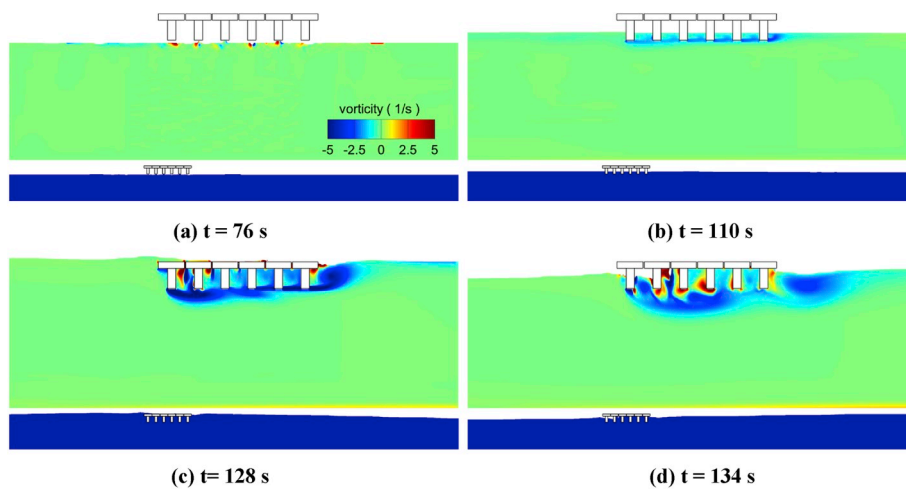
Fig. 31. The vorticity contours at different times at the submersion depth of 0.0 m.

Fig. 32c. When the wave leaves, there are still some vortices shedding from the bridge leading to the oscillation of the water. Although the water in the chambers oscillates strongly, wave propagation plays a dominant role in the change of the water level among girders. The deeper the immersion depth, the more obvious the turbulence phenomenon.

The temporal changes of horizontal and vertical forces on the bridges are recorded in Fig. 33. With the increase of submersion depth, both the maximum horizontal and vertical forces on the bridges decrease slightly because when the bridge immerses in the water, both the velocity around the bridge and the air pressure on the bridge decrease and the amount of water passing through the gap also greatly reduces. When the
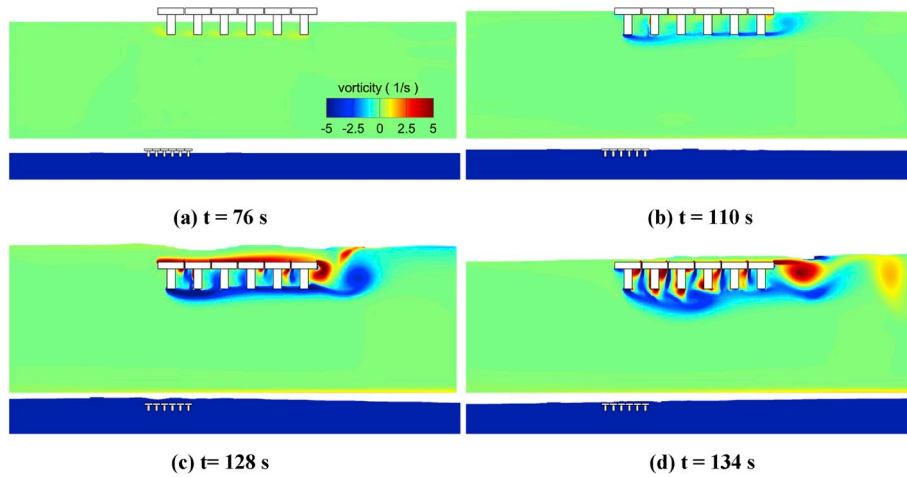
Fig. 32. The vorticity contours at different times at the submersion depth of 1.0 m.
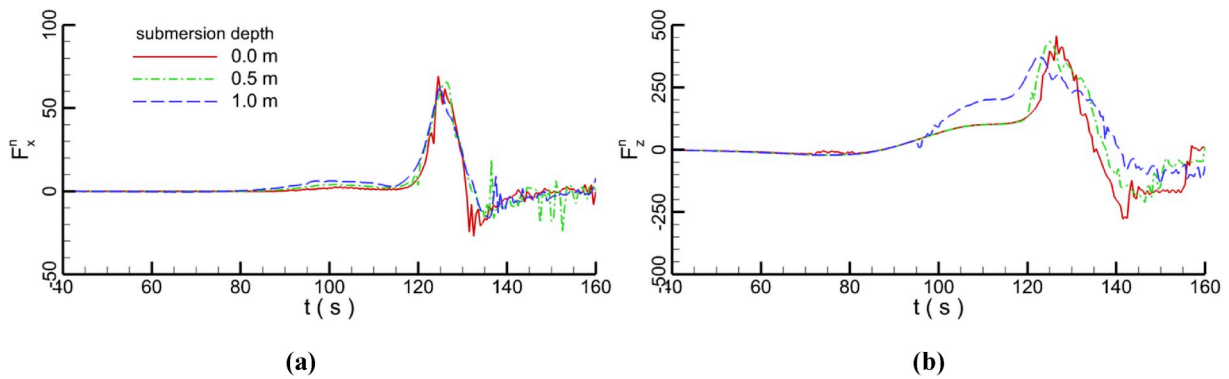
Fig. 33. The comparisons of the forces on the bridge with air vent under different submersion depths; (a) horizontal forces; (b) vertical forces.

water flows in the air vent, due to the mutual collision and water friction, both the flow energy and the overall flow velocity reduce, which weakens the force oscillation of bridges. After the wave leaves, the forces gradually reduce to the minimum. However, it is found that the submersion depth has a weak effect on the bridge with air vent.

5.4.4. The efficiency of air vent

Through the comparisons of hydrodynamic forces on the bridges with and without air vent, the efficiency of air vent on reducing the forces is investigated in this section. The force comparisons on different bridges with and without air vent are shown in Fig. 34. Although the locations of the bridges are different, the forces on the bridge without air vent are larger than that with air vent due to two reasons, firstly, if the air vent exists, the extra air pressure caused by the trapped air can be released through the air vent; secondly, around the air vent, the interaction between the rising water and flowing water on the bridge deck can reduce the wave energy and vertical force.

Depending on the maximum and minimum forces on the different bridges with and without air vent, the efficiency of the air vent is assessed using the comparison formula as

$$\nu = \frac{F_p^n - F_q^n}{F_p^n} \tag{17}$$

where ν is the efficiency coefficient, F_p^n and F_q^n represent the extreme values of forces on the bridge without and with air vent, respectively. The efficiency coefficients in different cases are shown in Fig. 35.

It is found that the values of the efficiency coefficients about the horizontal forces are very small, which means that the effect of the air

vent on the horizontal hydrodynamic forces is very weak. Compared with the horizontal efficiency coefficients, vertical coefficients are much larger because if the bridge does not have the air vent when the wave approaches the bridge, the air in the chamber is compressed and additional air pressure is generated to the bridge deck. The air pressure magnitudes on the front and rear surfaces of chamber are the same but the pressure directions are opposite. So, air pressure has little effect on the overall horizontal force of the bridge deck but exerts the very large vertical force on the horizontal plate of the bridge deck. When the air vent is in the bridge deck, as the water level rises, the air in the chamber is released through the air vent and the air pressure disappears. The vertical force is smaller than that on the bridge deck without air vent. With the increase of the submersion depth, the value of the coefficient decreases, indicating that the deeper the submersion depth, the less the impact of air vent on the bridge. The coefficients of the overall force magnitude on the bridge resemble that of maximum vertical forces because the vertical forces on the bridge account for the majority. The results demonstrate that the air vent has a great influence on the forces of the bridge, which can reduce the forces on the bridge to protect the bridge.

6. Conclusions

A numerical investigation about the effects of the tsunami-like wave on different bridge decks is conducted by applying incompressible flow solver with immersed boundary referred to IFS_IB. In the simulations, the effects of submersion depth, wave height and air vent on hydrodynamic loads on the bridge decks are analyzed. The main conclusions are drawn as follows.
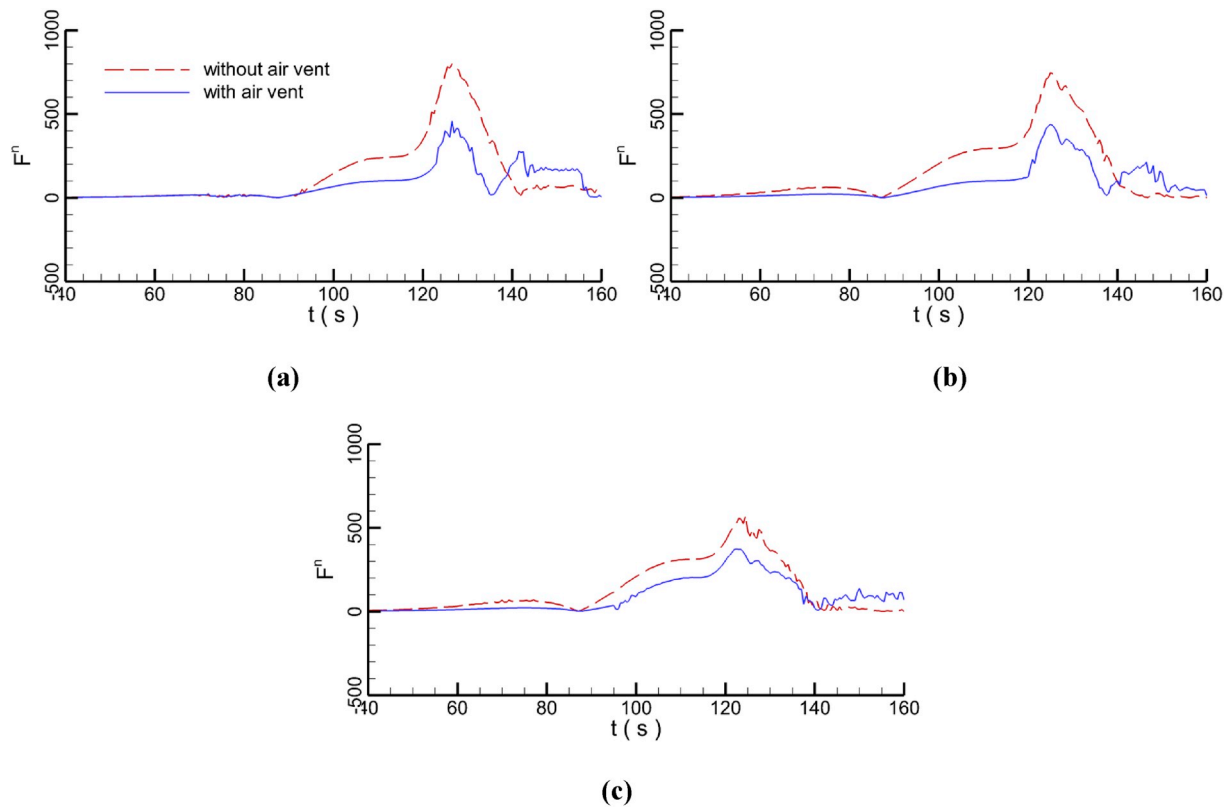
Fig. 34. The comparisons of dynamic forces on the bridge with and without air vents at different locations; (a) $S = 0.0$ m; (b) $S = 0.5$ m; (c) $S = 1.0$ m.
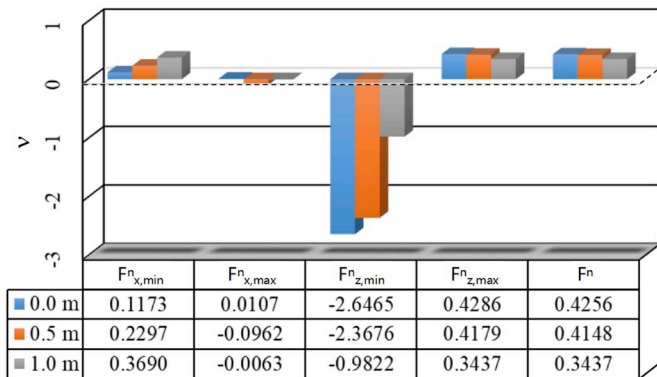
Fig. 35. The efficiency coefficients at different cases for the force extreme values.

1. When the tsunami-like wave passes over the bridge, the vertical forces on the bridges are larger than the horizontal forces, leading to many decks collapsed between two piers without lateral displacement after the hurricanes and tsunamis. After the tsunami-like wave passes over the bridge, the oscillation of the residual wave causes the load oscillation of the bridge. Compared with the solitary wave, the effect duration of tsunami-like wave on the bridge is much longer and the impact of this wave is also more serious. The results from comparisons between tsunami-like and solitary waves indicate that when studying the interaction between bridge and tsunami wave, tsunami wave cannot be simply simplified as solitary wave.

2. When the toe of the girder is above the still water surface initially, with the decrease of the bridge deck, both the horizontal and vertical forces on the bridge increase and the effect duration of the wave also extends. When a part of the bridge deck is under the free surface at the initial state, the horizontal forces on the bridges are similar to each other in different cases. As for the vertical forces, with the increase of the submersion depth, the forces decrease. The deeper the bridge is immersed, the smaller the vertical force on the bridge deck. When all the bridge deck has been immersed in the water before the tsunami-like wave peak arrives at the bridge deck, the bridge looks like a whole barrier to block the flow. The bigger vortices are generated and shed behind the bridge. With the increase of submersion depth, both the horizontal and vertical forces decrease.

3. With the increase of the wave height, the horizontal force magnitude increases, which basically shows a linear growth. The magnitude of the positive force is much larger than that of the negative force. Compared with the maximum horizontal forces, the vertical forces are much larger because the pressure caused by the rising water in the vertical direction is larger than that in the horizontal direction. In total, with the increase of the wave height, the interaction intensity between the tsunami-like wave and the bridge is enhanced and the forces on the bridge increase, but the effect duration reduces. The higher the wave height, the easier the bridge will be damaged.

4. When the bridge is with air vent, it has little influence on the horizontal force magnitude. After the wave passes over the bridge, the oscillation of the horizontal force on the bridge without air vent is more serious than that with air vent. However, the vertical force on the bridge with air vent is much less than that without air vent, which means that the air vent has a great influence on the vertical force. Due to the vertical force is much larger than the horizontal force, the vertical forces on the bridge account for the majority for the overall force. So, the air vent has a great impact on the overall force of bridge, which can reduce the forces on the bridge to protect the bridge.

This study can provide an assessment of tsunami wave forces on the different bridges. Large-scale physical experiments and the hydrodynamic characteristics around the bridge in real marine conditions are deserved to study in the future.

Declaration of competing interest

The authors declare that they have no known competing financial interests or personal relationships that could have appeared to influence the work reported in this paper.

CRediT authorship contribution statement

Enjin Zhao: Conceptualization, Methodology, Software, Investigation, Writing - original draft, Writing - review & editing. **Junkai Sun:** Data curation, Writing - original draft. **Yuezhao Tang:** Data curation, Writing - original draft. **Lin Mu:** Writing - review & editing. **Haoyu Jiang:** Writing - review & editing.

Acknowledgments

References

Chan, I.-C., Liu, P.L.-F., 2012. On the run-up of long waves on a plane beach. J. Geophys. Res. 117 (C8), 72–82. https://doi.org/10.1029/2012JC007994.

Cheng, Z.S., Gao, Z., Moan, T., 2018. Hydrodynamic load modelling and analysis of a floating bridge in homogenous wave conditions. Mar. Struct. 59, 122–141. https://doi.org/10.1016/j.marstruc.2018.01.007. https://www.sciencedirect.com/science/article/pii/S0951833917304094.

Crowley, R., Robeck, C., Dompe, P., 2018. A three-dimensional computational analysis of bridges subjected to monochromatic wave attack. J. Fluid Struct. 79, 76–93. https://doi.org/10.1016/j.jfluidstructs.2018.02.001. https://www.sciencedirect.com/science/article/pii/S0889974617300178?via%3Dihub.

Cuomo, G., Shimosako, K., Takahashi, S., 2009. Wave-in-deck loads on coastal bridges and the role of air. Coast Eng. 56 (8), 793–809. https://doi.org/10.1016/j.coastaleng.2009.01.005. https://www.sciencedirect.com/science/article/abs/pii/S0378383909000064.

Darwish, M., Moukalled, F., 2006. Convective schemes for capturing interfaces of free-surface flows on unstructured grids. Numer. Heat Tran., part B: Fundamentals. 49 (1), 19–42. https://doi.org/10.1080/10407790500272137. https://www_tandfonline.gg363.site/doi/abs/10.1080/10407790500272137.

Fang, Q.H., Hong, R.C., Guo, A., Stansby, P.K., Li, H., 2018. Analysis of hydrodynamic forces acting on submerged decks of coastal bridges under oblique wave action based on potential flow theory. Ocean. Eng. 169, 242–252. https://doi.org/10.1016/j.oceaneng.2018.09.031. https://www.sciencedirect.com/science/article/pii/S0029801818318456.

Goring, D.G., 1979. Tsunamis - the Propagation of Long Waves onto a Shelf. California. California Inst. of Technol. https://authors.library.caltech.edu/25987/1/KH-R-38.pdf.

Goseberg, N., Wurpts, A., Schlurmann, T., 2013. Laboratory-scale generation of tsunami and long waves. Coast Eng. 79, 57–74. https://doi.org/10.1016/j.coastaleng.2013.04.006. https://www.sciencedirect.com/science/article/pii/S0378383913000823?via%3Dihub.

Hayatdavoodi, M., Seiffert, B., Ertekin, R.C., 2014. Experiments and computations of solitary-wave forces on a coastal-bridge deck Part II: deck with girders. Coast Eng. 88, 210–228. https://doi.org/10.1016/j.coastaleng.2014.02.007. https://www.sciencedirect.com/science/article/abs/pii/S0378383914000398.

Hirt, C.W., Sicilian, J.M., 1985. A porosity technique for the definition of obstacles in rectangular cell meshes. 4th International Conference on Numerical Ship Hydrodynamics. https://trid.trb.org/view/394627.

Issa, R.I., 1986. Solution of the implicitly discretised fluid flow equations by operator-splitting. J. Comput. Phys. 62 (1), 40–65. https://doi.org/10.1016/0021-9991(86)90099-9. https://www.sciencedirect.com/science/article/pii/0021999186900999.

Liang, D.F., Gotoh, H., Khayyer, A., Chen, J.M., 2013. Boussinesq mdelling of solitary wave and N-wave runup on coast. Appl. Ocean Res. 42, 144–154. https://doi.org/10.1016/j.apor.2013.05.008. https://www.sciencedirect.com/science/article/pii/S0141118713000436.

Liang, D.F., Jian, W., Shao, S.D., Chen, R.D., Yang, K.J., 2017. Incompressible sph simulation of solitary wave interaction with movable seawalls. J. Fluid Struct. 69, 72–88. https://doi.org/10.1016/j.jfluidstructs.2016.11.015. https://www.sciencedirect.com/science/article/pii/S088997461630295X.

Madsen, P.A., Fuhrman, D.R., Schäffer, H.A., 2008. On the solitary wave paradigm for tsunamis. J. Geophys. Res.: Oceans 113 (C12), 286–292. https://doi.org/10.1029/2008JC004932. https://agupubs.onlinelibrary.wiley.com/doi/abs/10.1029/2008JC004932.

O'Connor, J.S., McAnany, P.E., 2008. Damage to engineered bridges from wind, storm surge and debris in the wake of hurricane Katrina. Earthquake Engineering to Extreme Events (MCEER) 8 (5), 9–119. http://www.buffalo.edu/mceer/catalog.host.html/content/shared/www/mceer/publications/MCEER-08-SP05.detail.html.

Qu, K., Ren, X.Y., Kraatz, S., Zhao, E.J., 2017a. Numerical analysis of tsunami-like wave impact on horizontal cylinders. Ocean. Eng. 145, 316–333. https://doi.org/10.1016/j.oceaneng.2017.09.027. https://www.sciencedirect.com/science/article/pii/S0029801817305462.

Qu, K., Ren, X.Y., Kraatz, S., 2017b. Numerical investigation of tsunami-like wave hydrodynamic characteristics and its comparison with solitary wave. Appl. Ocean Res. 63, 36–48. https://doi.org/10.1016/j.apor.2017.01.003.

Rossetto, T., Allsop, W., Charvet, I., Robinson, I.D., 2011. Physical modelling of tsunami using a new pneumatic wave generator. Coast Eng. 58, 517–527. https://doi.org/10.1016/j.coastaleng.2011.01.012. https://www.sciencedirect.com/science/article/pii/S0378383911000135?via%3Dihub.

Sarfaraz, M., Pak, A., 2017. SPH numerical simulation of tsunami wave forces impinged on bridge superstructures. Coast Eng. 121, 145–157. https://doi.org/10.1016/j.coastaleng.2016.12.005. https://www.sciencedirect.com/science/article/abs/pii/S0378383916304537.

Seiffert, B.R., Hayatdavoodi, M., Ertekin, R.C., 2015a. Experiments and calculations of conoidal wave loads on a coastal-bridge deck with girders. Eur. J. Mech. B Fluid 52, 191–205. https://doi.org/10.1016/j.euromechflu.2015.03.010. https://www.sciencedirect.com/science/article/abs/pii/S099775461500045X.

Seiffert, B.R., Ertekin, R.C., Robertson, I.N., 2015b. Wave loads on a coastal bridge deck and the role of entrapped air. Appl. Ocean Res. 53, 91–106. https://doi.org/10.1016/j.apor.2015.07.010. https://www.sciencedirect.com/science/article/abs/pii/S0141118715001042.

Synolakis, C.E., 1987. The run-up of solitary waves. J. Fluid Mech. 185, 523–545.

Wang, X., Zhou, J.F., Wang, Z., You, Y.X., 2018. A numerical and experimental study of internal solitary wave loads on semi-submersible platform. Coast Eng. 150, 298–308. https://doi.org/10.1016/j.oceaneng.2017.12.042. https://www.sciencedirect.com/science/article/pii/S0029801817307709.

Williams, I.A., Fuhrman, D.R., 2016. Numerical simulation of tsunami-scale wave boundary layers. Coast Eng. 110, 17–31. https://doi.org/10.1016/j.coastaleng.2015.12.002. https://www.sciencedirect.com/science/article/pii/S0378383915002100?via%3Dihub.

Winter, A.O., Motley, M.R., Eberhard, M.O., 2017. Tsunami-like wave loading of individual bridge components. J. Bridge Eng. 23 (2), 04017137 https://doi.org/10.1061/(ASCE)BE.1943-5592.0001177. https://ascelibrary.org/doi/abs/10.1061/%28ASCE%29BE.1943-5592.0001177.

Wu, Y.T., Yeh, C.L., Hsiao, S.C., 2014. Three-dimensional numerical simulation on the interaction of solitary waves and porous breakwaters. Coast Eng. 85, 12–29. https://doi.org/10.1016/j.coastaleng.2013.12.003. https://www.sciencedirect.com/science/article/pii/S0378383913002019?via%3Dihub.

Xiao, H., Huang, W., Chen, Q., 2010. Effects of submersion depth on wave uplift force acting on Biloxi Bay Bridge decks during Hurricane Katrina. Comput. Fluid 39 (8), 1390–1400. https://doi.org/10.1016/j.compfluid.2010.04.009. https://www.sciencedirect.com/science/article/pii/S004579301000085X.

Xu, G.J., Chen, Q., Chen, J.H., 2018. Prediction of solitary wave forces on coastal bridge decks using artificial neural networks. J. Bridge Eng. 23 (5), 04018023 https://doi.org/10.1061/(ASCE)BE.1943-5592.0001215. https://ascelibrary.org/doi/abs/10.1061/(ASCE)BE.1943-5592.0001215.

You, R., He, G.H., Wang, J.D., Liu, P.F., 2019. CIP-based analysis on strongly nonlinear interaction between solitary wave and submerged flat plate. Ocean. Eng. 176, 211–221. https://doi.org/10.1016/j.oceaneng.2019.02.050. https://www.sciencedirect.com/science/article/pii/S0029801818318031.

Zhao, M., Cheng, L., Teng, B., 2007. Numerical simulation of solitary wave scattering by a circular cylinder array. Ocean. Eng. 34, 489–499. https://doi.org/10.1016/j.oceaneng.2006.03.005. https://www.sciencedirect.com/science/article/pii/S0029801806001041.

Zhao, E.J., Qu, K., Mu, L., Kraatz, S., Shi, B., 2019a. Numerical study on the hydrodynamic characteristics of submarine pipelines under the impact of real-world Tsunami-like waves. Water 11 (2), 221. https://doi.org/10.3390/w11020221. https://www.mdpi.gg363.site/2073-4441/11/2/221.

Zhao, E.J., Qu, K., Mu, L., 2019b. Numerical study of morphological response of the sandy bed after tsunami-like wave overtopping an impermeable seawall. Ocean. Eng. 186, 106076. https://doi.org/10.1016/j.oceaneng.2019.05.058. https://www.sciencedirect.com/science/article/pii/S0029801819302793.

Zhao, E.J., Shi, B., Qu, K., Dong, W.B., Zhang, J., 2018. Experimental and numerical investigation of local scour around submarine piggyback pipeline under steady current. J. Ocean Univ. China 17 (2), 224–256. https://doi.org/10.1007/s11802-018-3290-7.

Zhao, E.J., Sun, J.K., Jiang, H.Y., Mu, L., 2019c. Numerical study on the hydrodynamic characteristics and responses of moored floating marine cylinders under real-world tsunami-like waves. IEEE Access 7, 122435–122458. https://doi.org/10.1109/ACCESS.2019.2934859. https://ieeexplore_ieee.gg363.site/abstract/document/8798482.